bring, C. R. Acad. Sci. Paris 270, 354 (1970).
[41]We wish to acknowledge the helpful discussions on the decay of ^{233}Th with Dr. Claire Sebille.
[42]B. E. Chi, Nucl. Phys. 83, 97 (1966); and State University of New York at Albany Report, 1967 (unpublished).
[43]S. G. Nilsson, C. F. Tsang, A. Sobiczewski, Z. Szymanski, S. Wycech, C. Gustavson, I.-L. Lamm, P. Möller, and B. Nilsson, Nucl. Phys. A131, 1 (1969).
[44]B. Nilsson, ϵ_4 Program, Program Library, Nordita, Copenhagen, (unpublished).
[45]L. A. Malov and V. G. Soloviev, Yadern. Fiz. 5, 566 (1967) [transl.: Soviet J. Nucl. Phys. 5, 403 (1967)].
[46]I. Ahmad, Argonne National Laboratory, private communication.
[47]K. Nybö, University of Bergen, Norway, private communication.
[48]T. von Egidy, Th. W. Elze, and J. R. Huizenga, Nucl. Phys. A145, 306 (1970).
[49]T. H. Braid, R. R. Chasman, J. R. Erskine, and A. M. Friedman, Phys. Letters 18, 149 (1965).
[50]B. Elbeck and P. O. Tjöm, in *Advances in Nuclear Physics*, edited by M. Baranger and E. Vogt (Plenum, New York, 1969), Vol. 3, p. 259.
[51]We are indebted to R. Santo and G. Gaul for providing the DWBA calculations.
[52]K. E. G. Löbner, M. Vetter, and V. Hönig, Nucl. Data A7, 495 (1970).
[53]J. M. Moss, Y. D. Terrien, R. M. Lombard, C. Brassard, J. M. Loiseaux, and F. Resmini, Phys. Rev. Letters 26, 1488 (1971).
[54]J. R. Erskine, Phys. Rev. C 5, 959 (1972).
[55]This code was developed by E. Sutter and J. R. Erskine.
[56]R. F. Casten, P. Kleinheinz, P. J. Daly, and B. Elbek, Phys. Rev. C 3, 1271 (1971).
[57]R. T. Brockmeier, S. Wahlborn, E. J. Seppi, and F. Boehm, Nucl. Phys. 63, 102 (1965).
[58]Th. W. Elze, T. von Egidy, and J. R. Huizenga, Nucl. Phys. A128, 564 (1969).
[59]J. S. Boyno, Th. W. Elze, and J. R. Huizenga, Nucl. Phys. A154, 263 (1970).
[60]T. H. Braid, R. R. Chasman, J. R. Erskine, and A. M. Friedman, unpublished.

PHYSICAL REVIEW C VOLUME 6, NUMBER 1 JULY 1972

Compound Spreading Widths for Bi^{209} Analog Resonances*

William P. Beres and David A. Voges
Department of Physics, Wayne State University, Detroit, Michigan 48202
(Received 7 January 1972)

The compound spreading widths (due to the Coulomb interaction) of $\frac{9}{2}^+$, $\frac{11}{2}^+$, $\frac{15}{2}^-$, $\frac{1}{2}^+$, $\frac{7}{2}^+$, and $\frac{3}{2}^+$ analog resonances in Bi^{209} are calculated within the general framework of the de Toledo Piza–Kerman scheme by relegating the giant isovector monopole contributions to the continuum space. The work emphasizes the structure of the parent states and the coupling is via $[H_c, T_-]$. The widths are found to be of the order of 20 keV, which is considerably less than the observed experimental total widths of 200–300 keV. A background of (i) configuration states (6 including the antianalog state for each analog resonance) and (ii) complex levels (e.g., 33 261 states for $\frac{9}{2}^+$ are considered. The one-body Coulomb interaction represented by a uniform sphere of charge is used for (i), while the two-body Coulomb force is expanded in multipoles for (ii). In (i) the dependence on the Coulomb radius and the nuclear spreading width are also studied. For all doorways the relative importance, number, density, strength, and compound-width contributions are investigated in great detail and the results are presented in tables and histograms. In addition to certain states of type (i) the most significant complex states are those based on the Pb^{208} giant dipole doorway resonance.

I. INTRODUCTION

The discovery of isobaric analog resonances as members of isobaric multiplets has led to much experimental and theoretical activity.[1] If, e.g., an analog resonance is formed by proton bombardment of a target nucleus (Z, N) with isospin quantum numbers (T, T), then the analog resonance is in the nucleus $(Z+1, N)$, and the quantum numbers are $(T+\frac{1}{2}, T-\frac{1}{2})$. This state is considered to be the second member of a $2T+2$ multiplet, the first member of which is the parent state $(T+\frac{1}{2}, T+\frac{1}{2})$. This level is a low-lying bound state in the adjacent parent nucleus $(Z, N+1)$. Isospin-violating forces (primarily the Coulomb repulsion among protons) remove the energy degeneracy of the multiplet members and shift the analog state upward into the continuum. In addition to this gross shift the isospin of the analog level ceases to be pure. The long-range Coulomb force results, however, in only weak coupling to the vast horde of neighboring states of lower isospin $(T-\frac{1}{2}, T-\frac{1}{2})$. We will

use the notation $T_> = T + \frac{1}{2}$ and $T_< = T - \frac{1}{2}$. The only isospin-violating force used in the present paper will be the Coulomb force alluded to above.

A study of analog resonances leads to information about the structure of the parent states and also target excited states. However, in the present paper our emphasis will be on an analysis of those compound states in the analog nucleus that contribute to the ultimate decay of the analog resonance. The portion of Hilbert space we will treat is the *compound* (or closed-channel) *space* $Q|\Psi\rangle$. The states in this space are orthogonal to those in the continuum (or open-channel) space $P|\Psi\rangle$, and to the analog space $A|\Psi\rangle$. In other words, if Q, P, and A are projection operators, then the total wave function $|\Psi\rangle$ is given as[2]

$$|\Psi\rangle = Q|\Psi\rangle + P|\Psi\rangle + A|\Psi\rangle . \tag{1}$$

A very important simple mode of excitation (the giant isovector monopole vibration) is not considered in the present calculation as part of the compound space. Mekjian[3] and Auerbach *et al.*[4] have indicated that states of that type are significant, and a calculation of monopole effects in the compound space is planned for the future.

Our aim is to calculate not only the effects of the $A|\Psi\rangle \rightarrow Q|\Psi\rangle$ couplings on the width of the analog state, but also to determine which background compound states are most relevant. We will investigate in much detail the structure of the seemingly complex array of compound space states embedded in the continuum. This work will verify that only certain of these states are important, viz: (i) those levels most strongly reached from the analog resonance by the Coulomb force, and (ii) those levels that are strongly weighted because of their proximity to the analog resonance. The states of type (i) are doorway states of the sort generally associated with the phenomenon of intermediate structure. Specifically, these will turn out to be the configuration states and levels related to the giant-dipole state. The configuration states are those $T_<$ levels generically related to the analog state itself, but located energetically considerably below the analog state because of the nuclear symmetry energy.

In performing this work the scheme of de Toledo Piza and Kerman[5] is used. This provides a natural separation of the structure and reaction theory problems, and allows us to use a simple nuclear model for the parent bound states and the levels in the analog nucleus compound space $Q|\Psi\rangle$. These compound states lead to what we will call following Kerman,[2] *compound mixing*. This is somewhat related to the internal mixing of Robson.[6] As part of the demonstration of doorway effects we will give for comparison the coupling matrix element results for many other complex levels whose presence, we shall see, contributes very little to the spreading width. The implication of this is that only certain carefully selected doorway states need be considered in future work.

The particular analog nucleus considered here is Bi^{209}, whose parent nucleus is Pb^{209}. This mass number is in a region that should possess strong shell effects and support the use of a shell-model description of the basic pertinent states. Section II will deal with the theory, Sec. III will give the results, and Sec. IV will discuss the results and summarize the main conclusions.

II. THEORY

A. Introduction

We first outline the essential steps leading to an expression for the compound spreading (or mixing) width Γ^{comp}. Let $|\Pi_i\rangle$ denote the ith state in the parent nucleus. Each such state is an actual eigenstate of the total Hamiltonian, i.e.,

$$H|\Pi_i\rangle = E_i|\Pi_i\rangle . \tag{2}$$

Although it is not necessary, for simplicity in this paper we will assume that $|\Pi_i\rangle$ is a state of good isospin $T_>$. The mixing of higher isospin into $|\Pi_i\rangle$ is quite small and does not add anything to the present analysis. We also assume that each $|\Pi_i\rangle$ is a single-neutron state. Configuration mixing in Pb^{209} should be sufficiently small to justify this. (Auerbach *et al.*[4] have found that such mixing makes extremely small corrections to Coulomb displacement energies in Sr^{89}.) It then follows that the ith analog state $|A_i\rangle$ is

$$|A_i\rangle = \frac{T_-|\Pi_i\rangle}{\langle\Pi_i|T_+T_-|\Pi_i\rangle^{1/2}} = \frac{T_-|\Pi_i\rangle}{\sqrt{2T+1}}, \tag{3}$$

where T_+ and T_- are the usual raising and lowering operator components of the total isospin operator. Because of isospin-violating terms the states $|A_i\rangle$ are not eigenstates of H.

The total width Γ of the analog state $|A\rangle$ with a particular spin and parity (for ease we drop the subscript i) is given by

$$\Gamma = \Gamma^{\text{comp}} + \Gamma^{\text{cont}} , \tag{4}$$

where Γ^{comp} is the width for decay to the compound space $Q|\Psi\rangle$ and Γ^{cont} is the width for decay to the continuum space $P|\Psi\rangle$. We will only be concerned with the compound spreading width Γ^{comp} in this paper. Specifically Γ^{comp} is defined[4] via

$$\sum_q \frac{\langle A|H|q\rangle\langle q|H|A\rangle}{E - E_q + iI/2} = \Delta^{\text{comp}} - i\frac{\Gamma^{\text{comp}}}{2}, \tag{5}$$

where $|q\rangle$ represents the qth state of energy E_q in the compound space $Q|\Psi\rangle$, and the quantity Δ^{comp} is the shift of the analog state. (This shift will not be calculated here.) The energy E satisfies

$$H|\Psi\rangle = E|\Psi\rangle, \tag{6}$$

and the quantity $E+I/2$ indicates an average over all compound-nuclear resonances with a Lorentzian weight factor of width I. In general, the averaging width or internal I must be at least as large as Γ^{comp}. If we assume that only certain (namely the simpler) compound states are significant for coupling to $|A\rangle$ and call these the doorway states, then we may approximate Eq. (5) by

$$\Delta^{\text{comp}} - i\frac{\Gamma^{\text{comp}}}{2} \approx \sum_d \frac{\langle A|H|d\rangle\langle d|H|A\rangle}{E - E_d + i\Gamma_d/2}, \tag{7}$$

where the sum is over the doorway states and Γ_d is the width of the dth doorway $|d\rangle$ due to nuclear interactions. We emphasize that neither the states q in Eq. (5) nor the doorways need be of good isospin. In the present calculation, however, the doorways are either pure or nearly pure $T_<$ states. Equation (7) assumes that the doorways are not strongly coupled to each other through the more complex configurations in the $Q|\Psi\rangle$ space.

The specific choice of doorways will be indicated later. These must all be orthogonal to each other and to $|A\rangle$. Only discrete states compose the set $|q\rangle$, and hence $|d\rangle$. Giant isovector monopole excitations are assumed to be in the space $P|\Psi\rangle$ (as indicated in Sec. I) and, hence, contribute to Γ^{cont} only. This is allowable, since Γ, the sum of the compound and continuum mixing (Eq. 4), is the only experimentally observable quantity.

Since $|d\rangle$ and $|A\rangle$ are orthogonal and $|\Pi\rangle$ (for ease we drop the subscript i) is an eigenstate of H, it follows that

$$\langle d|H|A\rangle = \frac{1}{\sqrt{2T+1}}\langle d|[H, T_-]|\Pi\rangle. \tag{8}$$

This matrix element will vanish unless there is an isospin-violating term in H; in the present paper this term is H_C, the two-body Coulomb force acting between protons, so that

$$H = H_{\text{nuc}} + H_C, \tag{9}$$

where H_{nuc} is the nuclear Hamiltonian. The Coulomb interaction is given by

$$H_C = \frac{1}{4}\sum_{i>j} \frac{e^2}{|\vec{r}_i - \vec{r}_j|}(1-\tau_z^i)(1-\tau_z^j), \tag{10}$$

with $\tau_z = 2t_z$. We note that the Coulomb force is long-range, spin-independent, and much weaker than the nuclear force. The commutator of H_C and T_- is of use and is given by

$$H_C^{(-)} = [H_C, T_-] = \frac{1}{4}\sum_{i>j} \frac{e^2}{|\vec{r}_i - \vec{r}_j|}[(1-\tau_z^i)\tau_-^j + (1-\tau_z^j)\tau_-^i], \tag{11}$$

where $\tau_- = \tau_x - i\tau_y$. Equation (11) represents a two-body force that changes a neutron-proton pair into a proton-proton pair. Equation (8) may be rewritten as

$$\langle d|H|A\rangle = \frac{1}{\sqrt{2T+1}}\langle d|H_C^{(-)}|\Pi\rangle, \tag{12}$$

where we have assumed for this paper that the nuclear forces are charge-independent. We may therefore rewrite Eq. (7) as

$$\Delta^{\text{comp}} - i\frac{\Gamma^{\text{comp}}}{2} = \frac{1}{2T+1}\sum_d \frac{\langle\Pi|H_C^{(+)}|d\rangle\langle d|H_C^{(-)}|\Pi\rangle}{E - E_d + i\Gamma_d/2}. \tag{13}$$

Here the definition of $H_C^{(+)}$ follows from that of $H_C^{(-)}$ in Eq. (11). For ease the equal sign is written in Eq. (13); however, we realize that this equation is only as valid as our approximations allow.

We wish to evaluate Γ^{comp} at the analog-state energy E_A; thus, $E = E_A$ in Eq. (13). The doorway widths Γ_d are, in general, functions of energy, and can sometimes be observed experimentally. However, we shall simplify the calculation by using a specific value of Γ_d for each particular doorway. The values employed depend on the nature of the doorways and are based on reasonable experimental and theoretical estimates of an upper limit for Γ_d at the doorway energies.[7,8] (These are given in Sec. III A 1.) The Γ_d values will of course be most valid when $|E_A - E_d|$ is small. Therefore

$$\Gamma^{\text{comp}} = \frac{1}{2T+1}\sum_d \Gamma_d \frac{\langle\Pi|H_C^{(+)}|d\rangle\langle d|H_C^{(-)}|\Pi\rangle}{(E_A - E_d)^2 + (\Gamma_d/2)^2}. \tag{14}$$

A simple way of interpreting this equation is to assume that each doorway is spread with a Lorentz shape about its shell-model energy with a width parameter Γ_d. This width represents in our model the spreading of the doorway state due to nuclear forces, and we shall refer to it as the doorway spreading width. The width Γ^{comp} is calculated at the analog resonance from the tails of the different Lorentzians.

B. Matrix Elements

It suffices to develop an expression for $\langle d|H_C^{(-)}|\Pi\rangle$ in Eq. (14), since the matrix element of $H_C^{(+)}$ fol-

lows directly from this. The parent state is

$$|\Pi\rangle = |n\Phi_0\rangle = |T+\tfrac{1}{2}, T+\tfrac{1}{2}\rangle , \tag{15}$$

where n denotes a neutron and $|\Phi_0\rangle$ is the target wave function

$$|\Phi_0\rangle = |T, T\rangle . \tag{16}$$

We assume a spin-zero target of doubly closed shells. In second quantization, if the neutron is in a shell-model state nlj, then

$$|\Pi\rangle = b_\epsilon^\dagger |\Phi_0\rangle , \tag{17}$$

where $b^\dagger$ is the neutron creation operator and ϵ denotes the set of quantum numbers nlj. Similarly we let $a_\epsilon^\dagger$ be the proton creation operator, and b_ϵ and a_ϵ be the corresponding neutron and proton annihilation operators.

In second quantization the Coulomb interaction Eq. (10) becomes

$$H_C = \tfrac{1}{4} \sum_{\alpha\beta\gamma\delta} \langle \alpha\beta | h_C | \delta\gamma \rangle_a a_\alpha^\dagger a_\beta^\dagger a_\gamma a_\delta , \tag{18}$$

with h_C representing the two-body Coulomb interaction for a system of two protons (this will be treated in detail in Sec. II C) and the subscript a indicates that antisymmetrization has been included. The isospin raising and lowering operators T_+ and T_- become, respectively, in second quantization

$$T_+ = \sum_\alpha b_\alpha^\dagger a_\alpha , \quad T_- = \sum_\alpha a_\alpha^\dagger b_\alpha , \tag{19}$$

so that, in particular, $H_C^{(-)}$ in Eq. (11) becomes

$$H_C^{(-)} = [H_C, T_-] = \tfrac{1}{2} \sum_{\alpha\beta\gamma\delta} \langle \alpha\beta | h_C | \delta\gamma \rangle_a a_\alpha^\dagger a_\beta^\dagger a_\gamma b_\delta . \tag{20}$$

Thus $\langle d | H_C^{(-)} | \Pi \rangle$ may be evaluated using Eqs. (17) and (20) for selected doorway states $|d\rangle$ in the analog nucleus.

We may see which types of doorways are possible by investigating the operator

$$H_C^{(-)} |\Pi\rangle \propto a_\alpha^\dagger a_\beta^\dagger a_\gamma b_\delta b_\epsilon^\dagger |\Phi_0\rangle , \tag{21}$$

requiring that the total angular momentum and parity must be that associated with the single-neutron state ϵ. It follows easily that the allowed doorways are of three types, viz: single-proton, 2p-1h, and 3p-2h. The single-proton and the neutron, proton, proton-hole class of 2p-1h states combine to form the pure $T_<$ configuration states mentioned in Sec. I. Thus the three classes of doorway states considered in this paper are: (i) 2p-1h states of the type two protons and a proton hole; (ii) 3p-2h states of the type two protons, a proton-hole, a neutron, and a neutron-hole; and (iii) configuration states. All of these states are orthogonal to the analog state and each other. We consider the matrix elements Eq. (8) of each in turn. To limit the scope of this paper we *neglect*

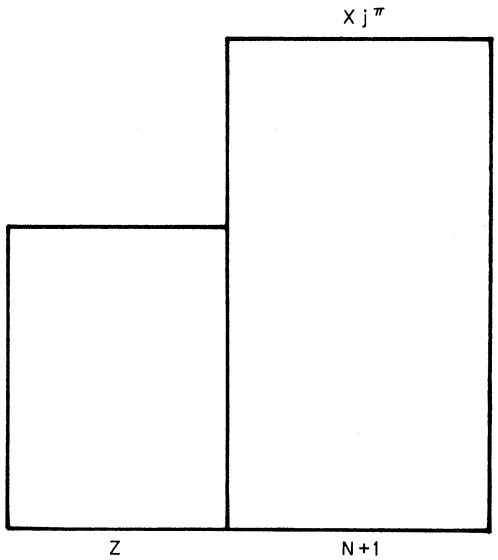

FIG. 1. Schematic shell-model picture of the parent state $|\Pi\rangle$ of spin and parity j^π in the nucleus with Z protons and $N+1$ neutrons. The nucleus (Z,N) is assumed to have doubly closed shells and j is shorthand for the quantum numbers nlj. The symbol × is for a particle.

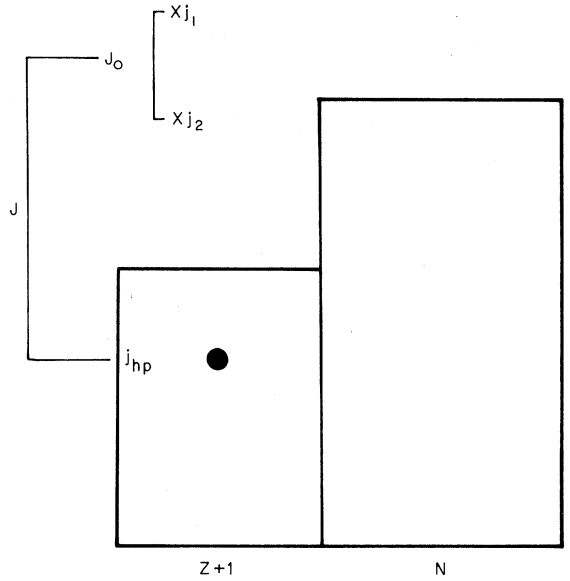

FIG. 2. Schematic shell-model picture of the doorway state $|2p\text{-}1h\rangle = |j_1 j_2 (J_0), j_{hp}; J^\pi M\rangle$ in the analog nucleus with $Z+1$ protons and N neutrons. The nucleus (Z,N) is assumed to have doubly closed shells and j is shorthand for the quantum numbers nlj. See Sec. II B 1 for additional details. The symbol × is for a particle and ● is for a hole.

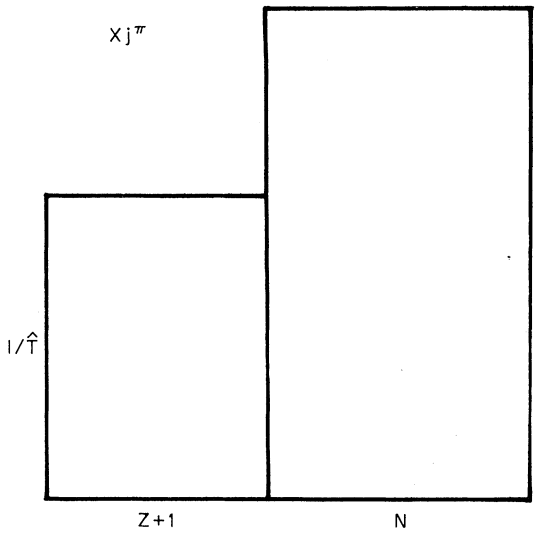

FIG. 3. Schematic shell-model picture of the single-proton part of the analog state wave function. The Coulomb coupling between this state and the doorway, Eq. (22), represents an alternate way of viewing the origin of the matrix element, Eq. (23). The symbol j is shorthand for the quantum numbers nlj. The symbol × is for a particle.

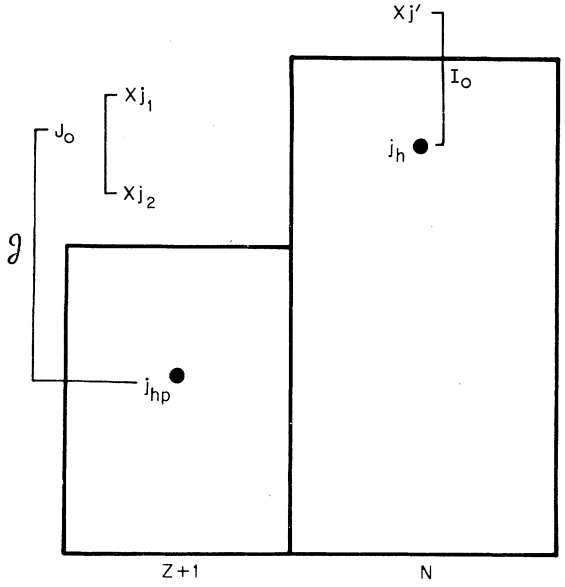

FIG. 4. Schematic shell-model picture of the doorway state $|3\text{p-}2\text{h}\rangle = (1+\delta_{n_1 n_2}\delta_{l_1 l_2}\delta_{j_1 j_2})^{-1/2} \times |[j_1 j_2(J_0), j_{hp}; \mathcal{J}][j' j_h(I_0)]J^\pi M\rangle$ in the analog nucleus with $Z+1$ protons and N neutrons. The nucleus (Z,N) is assumed to have doubly closed shells and j is shorthand for the quantum numbers nlj. See Sec. II B 2 for additional details. The symbol × is for a particle and ● is for a hole.

the mixing of different doorways with each other via either the Coulomb or the residual nuclear forces. This will mean, in particular, that there will be at certain energies many degenerate doorways of a particular type.

1. 2p-1h States

Each 2p-1h doorway state contains (as indicated in the last paragraph) three proton quasiparticles. Schematically the single-neutron parent state of angular momentum j and a typical $|2\text{p-}1\text{h}\rangle$ doorway level are indicated in Figs. 1 and 2, respectively. In Fig. 2, the two protons of angular momenta j_1 and j_2 and a proton-hole of angular momentum j_h couple to total angular momentum J. There are in general no restrictions as to whether none, one, or both of the protons are above the neutron excess as long as $J=j$ and the parities are the same. The coupling scheme selected for each $|2\text{p-}1\text{h}\rangle$ state is

$$|2\text{p-}1\text{h}\rangle = |j_1 j_2(J_0), j_{hp}; J^\pi M\rangle . \tag{22}$$

From Eq. (20), and Eqs. (17) and (22) (as illustrated in Figs. 1 and 2, respectively, and written in second quantization) the resultant matrix element Eq. (12) is

$$\begin{aligned}\langle d = 2\text{p-}1\text{h}\,|\,H\,|A\rangle &= \frac{1}{\hat{T}}\langle d = 2\text{p-}1\text{h}\,|\,H_C^{(-)}\,|\,\pi\rangle \\ &= \frac{1}{\hat{T}}(1+\delta_{j_1 j_2})^{-1/2}\frac{\hat{J}_0}{\hat{j}}\delta_{j^\pi J^\pi}\delta_{mM} \\ &\quad\times[\langle(j_{hp}j)J_0\,|\,h_C\,|\,(j_1 j_2)J_0\rangle \\ &\quad-(-1)^{j_1+j_2+J_0}\langle(j_{hp}j)J_0\,|\,h_C\,|\,(j_2 j_1)J_0\rangle],\end{aligned} \tag{23}$$

where m and M are the z projections of j and J, respectively, δ is the Kronecker δ, and the notation $\hat{j}=\sqrt{2j+1}$ is used. In the matrix elements of h_C the state j is that of a *proton*. When viewed entirely in the analog nucleus we recognize $1/\hat{T}$ times this state as the single-proton part of the analog resonance wave function, cf. Fig. 3. Thus we may view Eq. (23) as the Coulomb mixing of the doorway and the above-mentioned part of the analog state.

2. 3p-2h States

Each 3p-2h doorway state contains 3 proton quasiparticles and 2 neutron quasiparticles. In Fig. 4 a schematic picture of a typical such state is shown. Here the proton quasiparticles are represented by j_1, j_2, and j_{hp} and the neutrons by j' and j_h. Just as for the $|2\text{p-}1\text{h}\rangle$ doorways there are in general no restrictions on the proton states as long as $J^\pi = j^\pi$, where j^π is the parent state in Fig. 1. The coupling scheme selected for each $|3\text{p-}2\text{h}\rangle$

state is

$$|3p\text{-}2h\rangle = (1+\delta_{n_1n_2}\delta_{l_1l_2}\delta_{j_1j_2})^{-1/2} \times |[j_1j_2(J_0), j_{hp}; \mathcal{J}][j' j_h(I_0)]; J^\pi M\rangle. \quad (24)$$

From Eq. (20), and Eqs. (17) and (24) (as illustrated in Figs. 1 and 4, respectively, and written in second quantization) the resultant matrix element is [Eq. (12)]

$$\langle d=3p\text{-}2h\,|H|\,A\rangle = \frac{1}{\hat{T}}\langle d=3p\text{-}2h\,|H_C^{(-)}|\,\pi\rangle = \frac{\hat{j}_h}{\hat{T}}\frac{\hat{I}_0\hat{J}_0}{\hat{\mathcal{J}}}(-1)^{j'+j_h+I_0}(2j_h+1)^{-1}(1+\delta_{n_1n_2}\delta_{l_1l_2}\delta_{j_1j_2})^{-1/2}\delta_{\mathcal{J}^\pi j_h^\pi}\delta_{nn'} \times \delta_{l_1l'}\delta_{j_1j'}\delta_{j^\pi J^\pi}\delta_{mM}[\langle(j_{hp}j_h)J_0|h_C|(j_1j_2)J_0\rangle - (-1)^{j_1+j_2+J_0}\langle(j_{hp}j_h)J_0|h_C|(j_2j_1)J_0\rangle]. \quad (25)$$

In the matrix elements of h_C the state j_h is that of a *proton*. When viewed entirely in the analog nucleus, these matrix elements are due to the Coulomb mixing of the doorway with that 2p-1h (2 quasineutrons and 1 quasiproton) part of the analog-state wave function having both the proton particle and neutron hole in the state $n_hl_hj_h$ and coupled to 0^+. For this reason we have written $\hat{j}_h/\hat{T}$ as a separate factor in Eq. (25), it being just the amplitude of that part of the analog-state wave function of interest (cf. Fig. 5). The notation $\Phi_A(h)$ in Fig. 5 is defined below.

3. *Configuration States*

We consider these doorways as monopole excitations of the core *without* any change in the radial quantum number, and denote the ith configuration doorway (for a particular analog resonance) as $|\bar{A}_i\rangle$. The basis of states used to make the analog resonance wave function may be employed to generate the configuration states as a set of pure $T_<$ orthonormal levels. For a nucleus with a large neutron excess, there are neutrons in many different filled shells that can be transposed into protons in previously vacant proton shells. Thus the analog state in a heavy nucleus will have several 2p-1h terms and may be written as

$$|A\rangle = \frac{1}{\hat{T}}[|p\Phi_0\rangle + \sum_h \hat{j}_h|n\Phi_A(h)\rangle], \quad (26)$$

where T is as always the isospin of the doubly closed target whose wave function is $|\Phi_0\rangle$, p represents a proton of the same spin as the parent Eq. (15) and analog states, j_h is the spin of the tranposed neutron (cf. Fig. 5), and $\Phi_A(h)$ is the analog of $|\Phi_0\rangle$ obtained by converting the hth neutron into a corresponding proton. The symbol j_h is shorthand for the quantum numbers $n_hl_hj_h$ and the sum in Eq. (26) is over all the different excess neutron shells. In the case of only one excess neutron shell, $\hat{j}_h$ in Eq. (26) reduces to the familiar $\sqrt{2T}$.

While there are many different ways of constructing the configuration states,[7,9] we make them in the usual way by placing all of the single-proton strength in one state, viz., the *antianalog state*. This choice should not have much effect on our results. For example, in Sr^{89}, Auerbach *et al.*[4] found that coherent mixing of the antianalog state with other possible configuration states to form new configuration levels caused only a 2–4% change in the escape width. We shall spell out the specific configuration states of Bi^{209} and some matrix elements in Sec. III A 2. To keep with the usual notation in the literature we shall call the antianalog state $|\bar{A}\rangle$ and use the subscript i in $|\bar{A}_i\rangle$ only for the remaining configuration states.

C. Coulomb Interaction

1. *For the Matrix Elements Involving 2p-1h [Eq. (23)] and 3p-2h [Eq. (25)] States*

In general we are interested in a two-body matrix element of the type

$$\langle[j_a(1)j_b(2)]J_0|h_C|[j_C(1)j_d(2)]J_0\rangle,$$

where j_a indicates the proton state $n_al_aj_a$, etc. The interaction h_C is just

$$h_C = \frac{e^2}{|\vec{r}_1-\vec{r}_2|}, \quad (27)$$

with $+e$ the proton charge and $\vec{r}_1$ and $\vec{r}_2$ representing the vector positions of protons 1 and 2, respectively. Expanding in multipoles of order k we have

$$\frac{1}{|\vec{r}_1-\vec{r}_2|} = \sum_{k=0}^{\infty}\frac{r_<^k}{r_>^{k+1}}P_k(\cos\Omega_{12}), \quad (28)$$

where $r_< = \min(r_1, r_2)$, $r_> = \max(r_1, r_2)$, P_k is the Legendre polynomial of order k, and Ω_{12} is the solid angle between $\vec{r}_1$ and $\vec{r}_2$. Using spherical tensor algebra the resulting matrix element is

$$\langle[j_a(1)j_b(2)]J_0|h_C|[j_c(1)j_d(2)]J_0\rangle = e^2\sum_{k=0}^{\infty}R^k_{abcd}(-1)^{j_a+j_b+J_0}\begin{Bmatrix} J_0 & j_b & j_a \\ k & j_c & j_d\end{Bmatrix} \times\langle l_aj_a\|C^k\|l_cj_c\rangle\langle l_bj_b\|C^k\|l_dj_d\rangle, \quad (29)$$

where $\{\}$ denotes a 6-j symbol, the last two factors are reduced matrix elements, C^k is the spherical tensor related to the spherical harmonic Y^k via

$$C^k=[4\pi/(2k+1)]^{1/2}Y_k, \tag{30}$$

and R^k_{abcd} is the Slater integral, which, when expressed in terms of the radial wave functions u_a, etc., becomes

$$R^k_{abcd}=\int_0^\infty dr_2 u_b(r_2)u_d(r_2) \times\left[r_2{}^k\int_{r_1=r_2}^\infty dr_1\frac{1}{r_1{}^{k+1}}u_a(r_1)u_c(r_1) + \frac{1}{r_2{}^{k+1}}\int_0^{r_1=r_2}dr_1 r_1{}^k u_a(r_1)u_c(r_1)\right]. \tag{31}$$

2. *For the Matrix Elements Involving Configuration States*

Because of the complexity in calculating matrix elements involving all of the core protons, we neglect exchange terms and use a one-body Coulomb potential $V_C(r)$. Typically, then, we will have to calculate matrix elements of the type

$$\langle n_p l_p j_p|V_C(r)|n_p l_p j_p\rangle,$$

where $n_p l_p j_p$ is a certain proton state. The explicit expression for each matrix element $\langle d=\bar{A}_i$ or $\bar{A}|H_C^{(-)}|\Pi\rangle$ depends on the nucleus of interest and the particular configuration state wave function. The calculation of the matrix elements will be described in Sec. III A 2 for the case of Bi^{209}. For ease we use for $V_C(r)$ the Coulomb potential of a uniform sphere of charge with radius $R_C=r_C A^{1/3}$, i.e.,

$$V_C(r)=\frac{Ze^2}{2R_C}\left(3-\frac{r^2}{R_C{}^2}\right), \quad r<R_C; \qquad V_C(r)=Ze^2/r, \quad r>R_C. \tag{32}$$

The parameter r_C will be specified later.

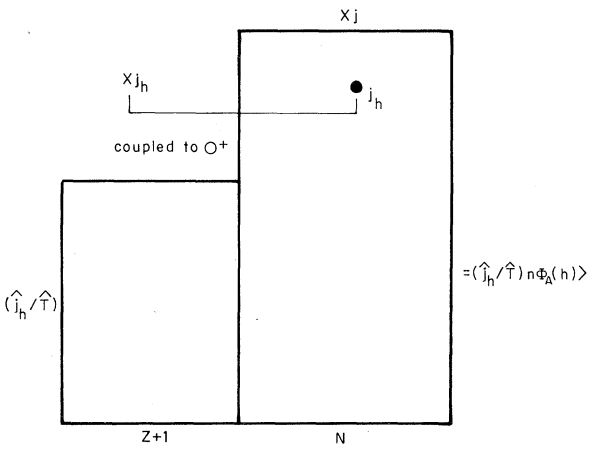

FIG. 5. The left-hand side of the equation represents a schematic shell-model picture of a particular 2p-1h (2 quasineutrons and 1 quasiproton) part of the analog-state wave function. The Coulomb coupling between this state and the 3p-2h doorway Eq. (24) represents an alternate way of viewing the origin of the matrix element Eq. (25). The symbol j is shorthand for the quantum numbers nlj. The right-hand side of the equation is discussed in Sec. II B 3. The symbol × is for a particle and ● is for a hole.

D. Compound Spreading Width Γ^{comp}

The expression Γ^{comp} in Eq. (14) for a particular analog resonance J^π may be rewritten in the form

$$\Gamma^{\text{comp}}=\sum_d \rho_d S_d, \tag{33}$$

where from Eqs. (12), (14), and (9),

$$S_d=|\langle d|H|A\rangle|^2=|\langle d|H_C|A\rangle|^2, \tag{34}$$

and from Eq. (14)

$$\rho_d=2\pi\,\frac{1}{2\pi}\left[\frac{\Gamma_d}{(E_A-E_d)^2+(\Gamma_d/2)^2}\right]. \tag{35}$$

The term S_d is the square of the Coulomb coupling matrix element and will be referred to as the *strength* of the doorway state $|d\rangle$. The coefficient ρ_d is 2π times the Lorentz distribution function of spreading width Γ_d described just after Eq. (14). We shall refer to ρ_d as the *density factor*. If there are several degenerate doorways at the energy E_d, then each will have the same density factor, but the strength of each will in general be different because of the difference between the doorway wave functions.

As discussed in Sec. II B, there are three different types of doorways, and we may accordingly write

$$\Gamma^{\text{comp}}=\Gamma^{\text{comp}}_{2\text{p-1h}}+\Gamma^{\text{comp}}_{3\text{p-2h}}+\Gamma^{\text{comp}}_{\text{config}}, \tag{36}$$

where

$$\Gamma^{\text{comp}}_{2\text{p-1h}}=\sum_d \Gamma^{\text{comp}}_{2\text{p-1h}}(d)=\sum_d \rho_{2\text{p-1h}}(d)S_{2\text{p-1h}}(d), \tag{37a}$$

$$\Gamma^{\text{comp}}_{3\text{p-2h}}=\sum_d \Gamma^{\text{comp}}_{3\text{p-2h}}(d)=\sum_d \rho_{3\text{p-2h}}(d)S_{3\text{p-2h}}(d), \tag{37b}$$

and

$$\Gamma^{\text{comp}}_{\text{config}}=\sum_d \Gamma^{\text{comp}}_{\text{config}}(d)=\sum_d \rho_{\text{config}}(d)S_{\text{config}}(d). \tag{37c}$$

The sums in Eqs. (37a)–(37c) are restricted, respectively, to doorways of the types 2p-1h, 3p-2h, and configuration states. Because the doorway

spreading widths are certainly not known for each individual doorway state, we use a different typical value of Γ_d for each of the three cases, viz. $\Gamma_{2p\text{-}1h}$, $\Gamma_{3p\text{-}2h}$, or Γ_{config}. (These will be specified in Sec. III.) Thus, for the dth doorway of each type the density factors are

$$\rho_{2p\text{-}1h}(d)=\frac{\Gamma_{2p\text{-}1h}}{(E_A-E_d)^2+(\Gamma_{2p\text{-}1h}/2)^2}, \tag{38a}$$

$$\rho_{3p\text{-}2h}(d)=\frac{\Gamma_{3p\text{-}2h}}{(E_A-E_d)^2+(\Gamma_{3p\text{-}2h}/2)^2}, \tag{38b}$$

and

$$\rho_{\text{config}}(d)=\frac{\Gamma_{\text{config}}}{(E_A-E_d)^2+(\Gamma_{\text{config}}/2)^2}. \tag{38c}$$

The strength S_d in Eq. (34) has been written as $S_{2p\text{-}1h}(d)$, $S_{3p\text{-}2h}(d)$, and $S_{\text{config}}(d)$ in Eqs. (37a)–(37c), respectively. The values of $S_{2p\text{-}1h}(d)$ and $S_{3p\text{-}2h}(d)$ are given, respectively, by the squares of Eqs. (23) and (25). The strength $S_{\text{config}}(d)$ will be obtained for the case of Bi^{209} in Sec. III.

III. RESULTS

A. Preliminaries

1. General

Here we will present the experimental and theoretical information necessary for the calculations. The target nucleus is Pb^{208} with 82 protons (assumed closed through the $3s_{1/2}$ shell) and 126 neutrons (assumed closed through the $3p_{1/2}$ shell). There are thus 44 excess neutrons, indicating an isospin of $T=22$ for Pb^{208}. In Fig. 6 the shell-model states used in the calculations are shown schematically in the order listed by Blomqvist and Wahlborn[10]; these states extend from $1g_{9/2}$ to $3d_{3/2}$ and include as excess neutron states the $1h_{9/2}$, $2f_{7/2}$, $1i_{13/2}$, $3p_{3/2}$, $2f_{5/2}$, and $3p_{1/2}$. The analog resonances considered in Bi^{209} are the $\frac{9}{2}^+$, $\frac{11}{2}^+$, $\frac{5}{2}^+$, $\frac{15}{2}^-$, $\frac{1}{2}^+$, $\frac{7}{2}^+$, and $\frac{3}{2}^+$ states whose respective single-neutron parents in Pb^{209} are the $2g_{9/2}$, $1i_{11/2}$, $3d_{5/2}$, $1j_{15/2}$, $4s_{1/2}$, $2g_{7/2}$, and $3d_{3/2}$ states. The order of the $1j_{15/2}$ and $3d_{5/2}$ neutron states is reversed in the summaries of Bromley and Weneser[11] and Stein[12] from that of Ref. 10. However the actual energies listed in Refs. 11 and 12 are not that much different from those of Ref. 10. Because many calculations have used the single-particle energies and Woods-Saxon well parameters given by Blomqvist and Wahlborn, and small energy errors will not effect our density factors or neutron wave functions significantly, we start with the energies of Ref. 10. The energy eigenvalues given in Ref. 10 are reproduced in Table I. In order to determine the missing energies needed to reproduce all the states of Fig. 6 we use the relationship between the proton energy E_p and the neutron energy E_n obtained by Pinkston[13] and Fallieros,[14] viz.,

$$E_p=E_n+(C-\delta)-E_{\text{sym}}, \tag{39}$$

where C is the Coulomb energy of the interaction of the proton with the core, δ is the n-p mass difference of 0.78 MeV, and E_{sym} is the nuclear symmetry energy, i.e., the energy difference between the analog resonance and its associated configuration states. From the experiment of Wharton *et al.*[15] the value of C is 18.79 MeV. The value of E_{sym} is taken as 11 MeV. MacFarlane and Schif-

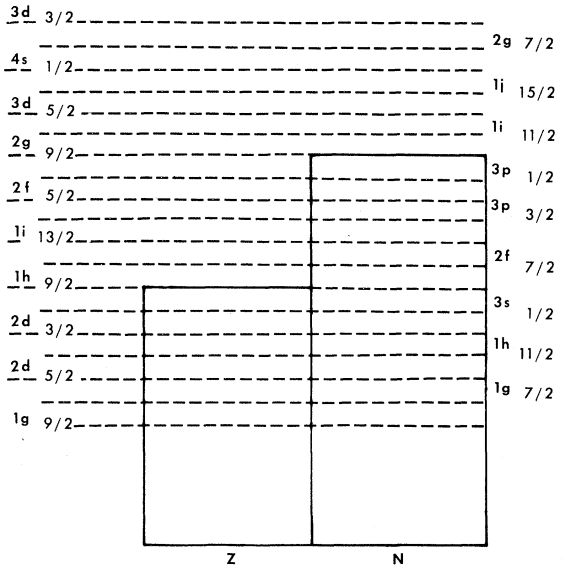

FIG. 6. Shell-model levels for neutrons and protons in Pb^{208} (Ref. 10).

TABLE I. Energy eigenvalues from Blomqvist and Wahlborn (Ref. 10). See Sec. III A 1 for details.

Neutron states		Proton states	
State	Energy in MeV	State	Energy in MeV
$3d_{3/2}$	−0.604	$3p_{1/2}$	Not bound
$2g_{7/2}$	−0.669	$2f_{5/2}$	Not bound
$4s_{1/2}$	−1.224	$3p_{3/2}$	Not bound
$1j_{15/2}$	−1.722	$1i_{13/2}$	−2.277
$3d_{5/2}$	−1.820	$2f_{7/2}$	−2.691
$1i_{11/2}$	−2.955	$1h_{9/2}$	−3.541
$2g_{9/2}$	−3.683		
$3p_{1/2}$	−7.232	$3s_{1/2}$	−7.032
$2f_{5/2}$	−7.986	$2d_{3/2}$	−7.515
$3p_{3/2}$	−8.130	$1h_{11/2}$	−8.663
$1i_{13/2}$	−8.429	$2d_{5/2}$	−9.346
$2f_{7/2}$	−10.279	$1g_{7/2}$	−11.064
$1h_{9/2}$	−10.797		

TABLE II. Single-particle energies used in the calculation. See Sec. III A 1 Eq. (39) and the text following for details. C=18.79 MeV, E_{sym}=11 MeV, δ=0.78 MeV.

State	E_n (MeV)	E_p (MeV)
$3d_{3/2}$	−0.60	6.41
$2g_{7/2}$	−0.67	6.34
$4s_{1/2}$	−1.22	5.79
$1j_{15/2}$	−1.72	5.29
$3d_{5/2}$	−1.82	5.19
$1i_{11/2}$	−2.96	4.06
$2g_{9/2}$	−3.68	3.33
$3p_{1/2}$	−7.23	−0.22
$2f_{5/2}$	−7.99	−0.98
$3p_{3/2}$	−8.13	−1.12
$1i_{13/2}$	−8.43	−1.42
$2f_{7/2}$	−10.28	−3.27
$1h_{9/2}$	−10.80	−3.79
$3s_{1/2}$	−14.03	−7.02
$2d_{3/2}$	−14.52	−7.51
$1h_{11/2}$	−15.66	−8.65
$2d_{5/2}$	−16.35	−9.34
$1g_{7/2}$	−18.06	−11.05
$1g_{9/2}$	−21.98	−14.97

fer[16] suggest a value of 10–11 MeV, while Mekjian[17] suggests 12 MeV. As a check, we calculate E_{sym} using Eq. (39) and the E_p and E_n values given in Table I for $1h_{9/2}$, $2f_{7/2}$, and $1i_{13/2}$. The average of the three resulting values of E_{sym} is about 11 MeV. Arbitrarily the $1h_{9/2}$ through $3p_{1/2}$ neutron energies were taken from Table I and the proton energies of these corresponding states were calculated using Eq. (39). Finally, the $1g_{9/2}$ energies are obtained with the help of Hamamoto.[18] The resulting neutron and proton energies used in the present paper are summarized in Table II. Also recorded are the values of δ, C, and E_{sym}.

The energies of the doorway states $|3(p)\rangle$, Eq. (22), and $|5(3p, 2n)\rangle$, Eq. (24), relative to threshold are obtained by adding the energies of the appropriate protons and neutrons in Table II. The energy difference between the $\frac{9}{2}^-$ ground state and threshold in Bi^{209} is taken as the experimental value of 3.72 MeV.[19] This must be added to the doorway energies if they are to be expressed relative to the ground state. The unmixed configuration states are all degenerate at an energy E_{sym} below the appropriate analog resonance energy. The center-of-mass energies of the analog resonances of interest are taken from Ref. 15 and are listed in Table III relative to threshold (i.e., Pb^{208} in its ground state with a proton at infinity) and also relative to the Bi^{209} ground state.

TABLE III. Analog state energies in Bi^{209} from Wharton *et al.* (Ref. 15).

Parent state in Pb^{209}	Analog state in Bi^{209}	Analog state energy in MeV for c.m. system relative to Threshold	Ground state
$2g_{9/2}$	$\frac{9}{2}^+$	14.847	18.57
$1i_{11/2}$	$\frac{11}{2}^+$	15.641	19.36
$1j_{15/2}$	$\frac{15}{2}^-$	16.258	19.98
$3d_{5/2}$	$\frac{5}{2}^+$	16.417	20.14
$4s_{1/2}$	$\frac{1}{2}^+$	16.884	20.60
$2g_{7/2}$	$\frac{7}{2}^+$	17.347	21.07
$3d_{3/2}$	$\frac{3}{2}^+$	17.392	21.11

Wave functions for all of the necessary single-particle states needed to evaluate matrix elements [Eqs. (23), (25), and also those involving configuration states] are obtained from a Woods-Saxon potential with spin-orbit coupling of the Thomas form. The single-*neutron* states in Table II are employed and the code ABACUS[20] is used to generate the wave functions. The expression for the potential is

$$V(r) = -V_0 f(r) - V_{so}\left(\frac{\hbar}{cm_\pi}\right)^2 \frac{1}{r}\frac{d}{dr} f(r)\vec{l}\cdot\vec{\sigma}\,, \tag{40a}$$

TABLE IV. Wave functions of the analog A, antianalog $\bar{A}$, and other configuration states $\bar{A}_i$. See Sec. III A 2 of the text.

State	Wave-function components $\|p\Phi_0\rangle$	$\|n\Phi_A(1h_{9/2})\rangle$	$\|n\Phi_A(2f_{7/2})\rangle$	$\|n\Phi_A(1i_{13/2})\rangle$	$\|n\Phi_A(2p_{3/2})\rangle$	$\|n\Phi_A(2f_{5/2})\rangle$	$\|n\Phi_A(3p_{1/2})\rangle$
A Eq. (41)	0.149	0.471	0.422	0.557	0.298	0.365	0.210
$\bar{A}$ Eq. (42)	0.988	−0.0711	−0.0635	−0.0841	−0.0449	−0.0550	−0.0318
$\bar{A}_1$	0	−0.190	−0.170	−0.224	0.759	−0.147	0.537
$\bar{A}_2$	0	0	0	0	−0.577	0	0.817
$\bar{A}_3$	0	−0.541	−0.484	0.576	0	0.378	0
$\bar{A}_4$	0	−0.667	0.746	0	0	0	0
$\bar{A}_5$	0	0	0	−0.548	0	0.837	0

TABLE V. Number of allowed doorway states in Bi^{209}.

J^π	$N_{2p-1h}=a$	N_{3p-2h} (h), where h is $1h_{9/2}$	$2f_{7/2}$	$1i_{13/2}$	$3p_{3/2}$	$2f_{5/2}$	$3p_{1/2}$	$N_{3p-2h}=b$ Eq. (48)	$N_{\text{config}}=c$	$N=a+b+c$ Eq. (47)
$\frac{9}{2}^+$	949	9380	7024	8770	2148	4428	562	32 312	6	33 267
$\frac{11}{2}^+$	938	9380	7024	10 524	2148	4428	562	34 066	6	35 010
$\frac{15}{2}^-$	768	9380	7024	12 278	2148	4428	562	35 820	6	36 594
$\frac{5}{2}^+$	749	5628	5268	5262	2148	4428	562	23 296	6	24 051
$\frac{1}{2}^+$	287	1876	1756	1754	1074	1476	562	8498	6	8791
$\frac{7}{2}^+$	884	7504	7024	7016	2148	4428	562	28 682	6	29 572
$\frac{3}{2}^+$	543	3752	3512	3508	2148	2952	562	16 434	6	16 983

with

$$f(r)=(1+e^{(r-R)/a})^{-1}, \tag{40b}$$

and

$$R=R_0A^{1/3}. \tag{40c}$$

The parameters $a=0.67$ fm, $R_0=1.27$ fm, and $V_{so}=7.75$ MeV are taken from Blomqvist and Wahlborn.[10] The suggested well depth V_0 is 44.0 MeV for all neutron states in Ref. 10. However, we have scanned over this parameter to obtain the best possible wave functions. The resulting well depths only differed by a maximum of about 2% from 44.0 MeV.

The doorway spreading widths Γ_{2p-1h} in Eq. (38a) and Γ_{3p-2h} in Eq. (38b) are taken, respectively, as 1 and 0.5 MeV as in the calculations of Refs. 7 and 8. We will mention the chosen values of Γ_{config} Eq. (38c) in Sec. III B 4 and discuss them in Sec. IV.

2. *Bi^{209} Configuration State Wave Functions and Matrix Elements*

First we write down the normalized wave function for the analog resonance using Eq. (26). The sum over h includes the six excess neutron shells, viz., $1h_{9/2}$, $2f_{7/2}$, $1i_{13/2}$, $3p_{3/2}$, $2f_{5/2}$, and $3p_{1/2}$, so that using $T=22$ we have

$$\begin{aligned}|A\rangle=\frac{1}{\sqrt{45}}[&|p\Phi_0\rangle+\sqrt{10}\,|n\Phi_A(1h_{9/2})\rangle+\sqrt{8}\,|n\Phi_A(2f_{7/2})\rangle\\&+\sqrt{14}\,|n\Phi_A(1i_{13/2})\rangle+\sqrt{4}\,|n\Phi_A(2p_{3/2})\rangle\\&+\sqrt{6}\,|n\Phi_A(2f_{5/2})\rangle+\sqrt{2}\,|n\Phi_A(3p_{1/2})\rangle].\end{aligned} \tag{41}$$

Because $|A\rangle$ has seven components there are six orthonormal configuration states that may be constructed. (These are unmixed and remain degenerate in our model at an energy $E_{sym}=11$ MeV below the analog resonance of interest.) We have purely arbitrarily used the coupling scheme which couples the excess neutrons together as follows: The isospins of the $1h_{9/2}$ and $2f_{7/2}$ excess neutrons are, respectively, 5 and 4. These are coupled to an isospin of 9. The isospins of the $1i_{13/2}$ and $2f_{5/2}$ excess neutrons are, respectively, 7 and 3. These are coupled to an isospin of 10. The total isospin of the $1h_{9/2}$, $2f_{7/2}$, $1i_{13/2}$, and $2f_{5/2}$ excess neutron shells is thus 19. The isospins of the $3p_{3/2}$ and $3p_{1/2}$ excess neutron shells are, respectively, 2 and 1. These are coupled to an isospin of 3. Finally, the total isospin of all the excess

TABLE VI. Compound mixing widths for analog resonances in Bi^{209} due to 2p-1h and 3p-2h states.

J^π	$\Gamma^{\text{comp}}_{2p-1h}=a$ (keV) Eq. (37a)	$\Gamma^{\text{comp}}_{3p-2h}(h)$ (keV) Eq. (49), where h is $1h_{9/2}$	$2f_{7/2}$	$1i_{13/2}$	$3p_{3/2}$	$2f_{5/2}$	$3p_{1/2}$	$\Gamma^{\text{comp}}_{3p-2h}=b$ (keV) Eqs. (50) or (37b)	$a+b$ (keV)
$\frac{9}{2}^+$	0.11	2.25	2.57	4.42	5.20	2.92	1.17	18.5	18.6
$\frac{11}{2}^+$	0.14	2.36	2.79	4.74	5.56	2.95	1.31	19.7	19.8
$\frac{15}{2}^-$	0.08	1.23	1.63	3.10	1.94	2.72	0.66	11.3	11.4
$\frac{5}{2}^+$	0.24	1.53	1.90	3.36	3.26	3.23	0.77	14.1	14.3
$\frac{1}{2}^+$	0.12	1.35	1.74	3.17	2.42	3.18	0.69	12.6	12.7
$\frac{7}{2}^+$	0.20	1.26	1.66	3.12	2.05	2.86	0.67	11.6	11.8
$\frac{3}{2}^+$	0.12	1.24	1.64	3.11	1.99	2.78	0.67	11.4	11.5

TABLE VII. Coulomb mixing strengths for analog resonances in Bi^{209} due to 2p-1h and 3p-2h states.

J^π	$S_{2p-1h}=a$ (10^4 keV^2) Eq. (54)	$S_{3p-2h}(h)$ (10^4 keV^2) Eq. (52), where h is $1h_{9/2}$	$2f_{7/2}$	$1i_{13/2}$	$3p_{3/2}$	$2f_{5/2}$	$3p_{1/2}$	$S_{3p-2h}=b$ (10^4 keV^2) Eq. (53)	$a+b$ (10^4 keV^2)
$\frac{9}{2}^+$	0.18								11.6
$\frac{11}{2}^+$	0.22								11.6
$\frac{15}{2}^-$	0.19	2.83 for each analog resonance	2.10 for each analog resonance	3.43 for each analog resonance	1.02 for each analog resonance	1.56 for each analog resonance	0.48 for each analog resonance	11.4 for each analog resonance	11.6
$\frac{5}{2}^+$	0.14								11.6
$\frac{1}{2}^+$	0.11								11.5
$\frac{7}{2}^+$	0.18								11.6
$\frac{3}{2}^+$	0.12								11.5

neutrons is $19+3=22$. Because of its special status (containing all the remaining single-proton strength) we spell out explicitly here the antianalog state (see also Ref. 21) as

$$|\bar{A}\rangle=\frac{1}{\sqrt{45}}\Big\{\sqrt{44}\,|p\Phi_0\rangle-\frac{1}{\sqrt{22}}[\sqrt{5}\,|n\Phi_A(1h_{9/2})\rangle+\sqrt{4}\,|n\Phi_A(2f_{7/2})\rangle+\sqrt{7}\,|n\Phi_A(1i_{13/2})\rangle+\sqrt{2}\,|n\Phi_A(2p_{3/2})\rangle+\sqrt{3}\,|n\Phi_A(2f_{5/2})\rangle+|n\Phi_A(3p_{1/2})\rangle]\Big\}. \tag{42}$$

In Table IV we summarize the analog and resulting configuration state wave functions. The first column lists the symbol for the state, i.e., A denotes analog, $\bar{A}$ means antianalog, and $\bar{A}_1,\ldots,\bar{A}_5$ represent the remaining configuration states. The other columns list the wave-function components of the basis states $|p\Phi_0\rangle$, $|n\Phi_A(1h_{9/2})\rangle,\ldots,$ and $|n\Phi_A(3p_{1/2})\rangle$.

TABLE VIII. Strengths of the configuration state doorways [*not including* the *antianalog* state Eq. (42)].

r_C (fm) Eq. (32)	$S_{config}(d)$ (10^4 keV^2), where d is (Table IV) $\bar{A}_1$	$\bar{A}_2$	$\bar{A}_3$	$\bar{A}_4$	$\bar{A}_5$	$\sum_{i=1}^{5} S_{config}(d=\bar{A}_i)$ (10^4 keV^2)
1.15	2.82	0.02	13.5	0.25	19.8	36.4
1.20	1.62	0.01	10.8	0.08	15.1	27.6
1.25	0.94	0.01	8.50	0.02	11.7	21.2
1.30	0.55	0.01	6.73	0.00	9.16	16.5
1.341 [a]	0.36	0.01	5.57	0.00	7.57	13.5
1.40	0.21	0.01	4.26	0.00	5.84	10.3

[a] The awkward value of $r_C=1.341$ fm is tried, since it was obtained in an O^{16} study by W. Beres and W. M. MacDonald, Nucl. Phys. 91, 529 (1967).

The necessary matrix elements, Eq. (12), become

$$\langle d=\bar{A}|H|A\rangle=\frac{1}{\hat{T}}\langle d=\bar{A}|H_C^{(-)}|\Pi\rangle=\langle\bar{A}|V_C(r)|A\rangle \tag{43}$$

for the antianalog state, and

$$\langle d=\bar{A}_i|H|A\rangle=\frac{1}{\hat{T}}\langle d=\bar{A}_i|H_C^{(-)}|\Pi\rangle=\langle\bar{A}_i|V_C(r)|A\rangle, \tag{44}$$

for the other configuration states, where $V_C(r)$ is the one-body Coulomb potential given by Eq. (32). Using the orthogonality of the different basis components in Eqs. (41) and (42), Eq. (43) becomes

$$\frac{1}{\hat{T}}\langle d=\bar{A}|H_C^{(-)}|\Pi\rangle=\frac{1}{45}\Big\{\sqrt{44}\,\langle p|V_C(r)|p\rangle-\frac{1}{\sqrt{22}}[\sqrt{50}\,\langle 1h_{9/2}|V_C(r)|1h_{9/2}\rangle+\sqrt{32}\,\langle 2f_{7/2}|V_C(r)|2f_{7/2}\rangle+\sqrt{98}\,\langle 1i_{13/2}|V_C(r)|1i_{13/2}\rangle+\sqrt{8}\,\langle 3p_{3/2}|V_C(r)|3p_{3/2}\rangle+\sqrt{18}\,\langle 2f_{5/2}|V_C(r)|2f_{5/2}\rangle+\sqrt{2}\,\langle 3p_{1/2}|V_C(r)|3p_{1/2}\rangle]\Big\}, \tag{45}$$

where p is the proton state defined in Eq. (26), and $1h_{9/2},\ldots,3p_{1/2}$ are the proton states corresponding to the respective neutron holes. The matrix elements Eq. (44) may be easily evaluated via Table IV. For example, one of the simpler results is

$$\langle d=\bar{A}_2|H_C^{(-)}|\Pi\rangle=0.172\,[-\langle 3p_{3/2}|V_C(r)|3p_{3/2}\rangle+\langle 3p_{1/2}|V_C(r)|3p_{1/2}\rangle]. \tag{46}$$

The square of the matrix element Eq. (43) gives the antianalog strength $S_{\text{config}}(d=\bar{A})$, and the square of each matrix element Eq. (44) yields the strength of each of the other configuration states, i.e., $S_{\text{config}}(d=\bar{A}_i)$. In Eq. (37c) these strengths may be used to calculate the compound spreading width due to the configuration states, i.e., $\Gamma^{\text{comp}}_{\text{config}}$. The Coulomb radius parameter r_C in $V_C(r)$ of Eq. (32) is taken as the reasonable value of 1.2 fm[7,22]; however, the results of altering r_C will also be indicated (Sec. III B 4).

B. Calculations

1. *Number of Doorway States*

The total number of possible doorway states N_{tot} may be written as

$$N_{\text{tot}} = N_{2p\text{-}1h} + N_{3p\text{-}2h} + N_{\text{config}}, \tag{47}$$

TABLE IX. Strengths of the configuration doorways *(including the antianalog state)* for each analog resonance.

J^π	E_{con} (MeV) (relative to ground state)	r_C (fm) Eq. (32)	$S_{\text{config}}(d=\bar{A})=a$ (10^4 keV^2)	$\sum_{i=1}^{5} S_{\text{config}}(d=\bar{A}_i)=b$ (10^4 keV^2) (Table VIII)	$S_{\text{config}}=a+b$ Eq. (55)
$\frac{9}{2}^+$	7.57	1.15	1.1	36.4	37.5
		1.20	1.00	27.6	28.6
		1.25	0.95	21.2	22.1
		1.30	0.86	16.5	17.3
		1.341	0.78	13.5	14.3
		1.40	0.7	10.3	11.0
$\frac{11}{2}^+$	8.36	1.15	0.35	36.4	36.8
		1.20	0.25	27.6	27.8
		1.25	0.18	21.2	21.4
		1.30	0.14	16.5	16.6
		1.341	0.11	13.5	13.6
		1.40	0.09	10.3	10.4
$\frac{15}{2}^-$	8.98	1.15	5.46	36.4	41.9
		1.20	4.38	27.6	32.0
		1.25	3.52	21.2	24.7
		1.30	2.84	16.5	19.3
		1.341	2.39	13.5	15.9
		1.40	1.87	10.3	12.2
$\frac{5}{2}^+$	9.14	1.15	5.84	36.4	42.3
		1.20	5.77	27.6	33.4
		1.25	5.54	21.2	26.7
		1.30	5.19	16.5	21.6
		1.341	4.84	13.5	18.4
		1.40	4.29	10.3	14.6
$\frac{1}{2}^+$	9.60	1.15	19.2	36.4	55.6
		1.20	18.5	27.6	46.1
		1.25	17.5	21.2	38.7
		1.30	16.3	16.5	32.8
		1.341	15.2	13.5	28.7
		1.40	13.6	10.3	23.9
$\frac{7}{2}^+$	10.07	1.15	2.51	36.4	39.0
		1.20	2.37	27.6	30.0
		1.25	2.18	21.2	23.4
		1.30	1.96	16.5	18.4
		1.341	1.78	13.5	15.3
		1.40	1.53	10.3	11.8
$\frac{3}{2}^+$	10.11	1.15	15.6	36.4	52.0
		1.20	14.9	27.6	42.5
		1.25	14.0	21.2	35.2
		1.30	12.9	16.5	29.4
		1.341	12.0	13.5	25.5
		1.40	11.2	10.3	21.5

with $N_{2p\text{-}1h}$, $N_{3p\text{-}2h}$, and N_{config} denoting, respectively, the number of *allowed* doorways of the 2p-1h [Eq. (22)], 3p-2h [Eq. (24)], and configuration (Table IV) types. (An allowed state is one that has the same spin and parity as the analog level of interest.) It is convenient to write $N_{3p\text{-}2h}$ in terms of each contribution $N_{3p\text{-}2h}(h)$ which represents the number of 3p-2h doorways having in common the same neutron hole $n_h l_h j_h$, i.e.,

$$N_{3p\text{-}2h}=\sum_h N_{3p\text{-}2h}(h), \tag{48}$$

where the sum is over all the excess neutron shells. Table V summarizes for each analog resonance listed in column 1 the value of $N_{2p\text{-}1h}$ in column 2, $N_{3p\text{-}2h}(h)$ in columns 3–8, $N_{3p\text{-}2h}$ [Eq. (48)] in column 9, N_{config} in column 10, and N_{tot} [Eq. (47)] in column 11.

2. Compound Spreading Widths Due to 2p-1h and 3p-2h Doorway States

It is convenient to rewrite $\Gamma^{comp}_{3p\text{-}2h}$ [Eq. (37b)] in terms of each contribution $\Gamma_{3p\text{-}2h}(h)$ which represents the width due to those 3p-2h doorways having in common the same neutron hole $n_h l_h j_h$, i.e.,

$$\Gamma^{comp}_{3p\text{-}2h}(h)=\sum_{d(h)}\Gamma^{comp}_{3p\text{-}2h}(d), \tag{49}$$

with $d(h)$ indicating that the sum is over the aforementioned doorway. Thus,

$$\Gamma^{comp}_{3p\text{-}2h}=\sum_h\Gamma^{comp}_{3p\text{-}2h}(h), \tag{50}$$

where as in Eq. (48), the sum is over all the neutron excess shells. In obtaining Eq. (50) we have used the fact from Eqs. (37b) and (49) that

$$\sum_d\Gamma^{comp}_{3p\text{-}2h}(d)=\sum_h\sum_{d(h)}\Gamma^{comp}_{3p\text{-}2h}(d). \tag{51}$$

In Table VI we summarize for each analog resonance listed in column 1 the value of $\Gamma^{comp}_{2p\text{-}1h}$ [Eq. (37a)] in column 2, $\Gamma^{comp}_{3p\text{-}2h}(h)$ [Eq. (49)] in columns 3–8, $\Gamma^{comp}_{3p\text{-}2h}$ [Eqs. (50) or (37b)] in column 9, and $\Gamma^{comp}_{2p\text{-}1h}+\Gamma^{comp}_{3p\text{-}2h}$ in column 10. All width values are given in keV.

3. Strengths of 2p-1h and 3p-2h Doorway States

By analogy to Eq. (49) we also define

$$S_{3p\text{-}2h}(h)=\sum_{d(h)}S_{3p\text{-}2h}(d), \tag{52}$$

where $S_{3p\text{-}2h}(d)$ is the strength defined in Eq. (37b) and discussed in Sec. II D, and $S_{3p\text{-}2h}(h)$ is the total strength due to all those allowed 3p-2h doorways associated with a particular neutron hole $n_h l_h j_h$. In addition we may write by analogy to Eqs. (50) and (51),

$$S_{3p\text{-}2h}=\sum_h S_{3p\text{-}2h}(h). \tag{53}$$

Here $S_{3p\text{-}2h}$ is the total strength for all the allowed 3p-2h doorways. For 2p-1h doorways we may define

$$S_{2p\text{-}1h}=\sum_d S_{2p\text{-}1h}(d) \tag{54}$$

as the total strength for all the allowed 2p-1h doorways. The term $S_{2p\text{-}1h}(d)$ is defined in Eq. (37a) and discussed in Sec. II D. Table VII presents for each analog resonance listed in column 1 the value of $S_{2p\text{-}1h}$ [Eq. (54)] in column 2, $S_{3p\text{-}2h}(h)$ [Eq. (52)] in columns 3–8, $S_{3p\text{-}2h}$ [Eq. (53)] in column 9, and $S_{2p\text{-}1h}+S_{3p\text{-}2h}$ in column 10. The reason why each value of $S_{3p\text{-}2h}(h)$ and also $S_{3p\text{-}2h}$ are the same for each analog resonance will be examined in Sec. III B 4.

4. Compound Spreading Widths and Strengths Due to the Configuration States

The total strength for all the configuration states S_{config} is given by

$$S_{config}=\sum_d S_{config}(d), \tag{55}$$

TABLE X. Compound spreading widths of analog resonances in Bi^{209} *due to all but the antianalog state.*

	$\Gamma^{comp}_{config}(d)$ (keV) Eq. (56), where d is (Table IV)										$\sum_{i=1}^{5}\Gamma^{comp}_{config}(d=\bar{A}_i)$ (keV)	
	$\bar{A}_1$		$\bar{A}_2$		$\bar{A}_3$		$\bar{A}_4$		$\bar{A}_5$			
r_C (fm) Eq. (32)	Ref. a	Ref. b	Ref. a	Ref. b	Ref. a	Ref. b	Ref. a	Ref. b	Ref. a	Ref. b	Ref. a	Ref. b
1.15	0.23	1.09	0.00	0.00	1.12	5.32	0.02	0.10	1.63	7.75	3.00	14.26
1.20	0.13	0.62	0.00	0.00	0.89	4.24	0.01	0.05	1.25	5.95	2.28	10.86
1.25	0.08	0.38	0.00	0.00	0.70	3.34	0.00	0.00	0.96	4.57	1.74	8.29
1.30	0.05	0.24	0.00	0.00	0.56	2.66	0.00	0.00	0.76	3.62	1.37	6.52
1.341	0.03	0.14	0.00	0.00	0.46	2.19	0.00	0.00	0.62	2.95	1.11	5.28
1.40	0.02	0.10	0.00	0.00	0.35	1.67	0.00	0.00	0.48	2.28	0.85	4.05

[a] $\Gamma_{config}=1$ MeV in Eq. (57), giving $\rho_{config}=8.24\times10^{-3}$ MeV^{-1}.
[b] $\Gamma_{config}=5$ MeV in Eq. (57), giving $\rho_{config}=3.92\times10^{-2}$ MeV^{-1}.

TABLE XI. Compound spreading widths due to all configuration states Γ^{comp}_{config} for analog resonances in Bi^{209}. Also listed are the compound spreading widths due to only the antianalog state Γ^{comp}_{config} $(d=\bar{A})$.

J^π	E_{con} (MeV) relative to ground state	r_C (fm) Eq. (32)	$\Gamma^{comp}_{config}(d=\bar{A})$ (keV) $\bar{A}$ is given by Eq. (42) and Table IV Ref. a	Ref. b	Γ^{comp}_{config} (keV) Eq. (58) Ref. a	Ref. b
$\frac{9}{2}^+$	7.57	1.15	0.09	0.43	3.09	14.7
		1.20	0.08	0.38	2.36	11.2
		1.25	0.08	0.38	1.82	8.67
		1.30	0.07	0.33	1.44	6.85
		1.341	0.06	0.29	1.17	5.57
		1.40	0.06	0.29	0.91	4.34
$\frac{11}{2}^+$	8.36	1.15	0.03	0.14	3.03	14.4
		1.20	0.02	0.10	2.30	11.0
		1.25	0.02	0.10	1.76	8.39
		1.30	0.01	0.05	1.38	6.57
		1.341	0.01	0.05	1.12	5.33
		1.40	0.01	0.05	0.86	4.10
$\frac{15}{2}^-$	8.98	1.15	0.45	2.24	3.45	16.4
		1.20	0.36	1.71	2.64	12.6
		1.25	0.29	1.38	2.03	9.65
		1.30	0.23	1.09	1.60	7.61
		1.341	0.20	0.95	1.31	6.24
		1.40	0.15	0.71	1.00	4.76
$\frac{5}{2}^+$	9.14	1.15	0.48	2.28	3.48	16.6
		1.20	0.48	2.28	2.76	13.1
		1.25	0.46	2.18	2.20	10.5
		1.30	0.43	2.04	1.80	8.56
		1.341	0.40	1.90	1.51	7.18
		1.40	0.35	1.66	1.20	5.71
$\frac{1}{2}^+$	9.60	1.15	1.59	7.56	4.59	21.8
		1.20	1.53	7.29	3.81	18.2
		1.25	1.45	6.90	3.19	15.2
		1.30	1.35	6.42	2.72	12.9
		1.341	1.26	6.00	2.37	11.3
		1.40	1.12	5.33	1.97	9.38
$\frac{7}{2}^+$	10.07	1.15	0.21	1.00	3.21	15.3
		1.20	0.20	0.95	2.48	11.8
		1.25	0.18	0.86	1.92	9.15
		1.30	0.16	0.76	1.53	7.28
		1.341	0.15	0.71	1.26	5.99
		1.40	0.13	0.62	0.98	4.67
$\frac{3}{2}^+$	10.11	1.15	1.28	6.10	4.28	20.4
		1.20	1.23	5.85	3.51	16.7
		1.25	1.15	5.47	2.89	13.8
		1.30	1.07	5.10	2.44	11.6
		1.341	0.99	4.71	2.10	9.99
		1.40	0.92	4.38	1.77	8.43

[a] $\Gamma_{config}=1$ MeV in Eq. (57), giving $\rho_{config}=8.24\times10^{-3}$ MeV^{-1}.
[b] $\Gamma_{config}=5$ MeV in Eq. (57), giving $\rho_{config}=3.92\times10^{-2}$ MeV^{-1}.

where $S_{\text{config}}(d)$ is defined in Eq. (37c). The sum over d is restricted to configuration doorways and in the case of Bi^{209} these are the six configuration states listed in Table IV. The strengths for five of these states [all but the antianalog state Eq. (42)] are independent of the total angular momentum, parity, and energy of the analog resonance and are given by the square of the matrix element Eq. (44). These strengths are listed in columns 2–6 of Table VIII for a range of values in column 1 of the Coulomb radius parameter r_C [Eq. (32)]. The sum of the five strengths for each r_C value is given in the last column. In Table IX for each analog resonance listed in column 1, and for the same range of values of r_C (column 3), the strength of each antianalog state $S_{\text{config}}(d=\bar{A})$ [the square of the matrix element Eq. (43)] is written in column 4. The values of $S_{\text{config}}(\bar{A})$ are added to the remaining configuration strengths (column 5) to yield the resultant values of S_{config} in column 6. In addition, for each analog state the energy E_{con} of the degenerate configuration states is given in column 2 relative to the ground state of Bi^{209}.

The width $\Gamma^{\text{comp}}_{\text{config}}(d)$ in Eq. (37c) may be written as

$$\Gamma^{\text{comp}}_{\text{config}}(d)=\rho_{\text{config}}S_{\text{config}}(d), \tag{56}$$

where ρ_{config} is the same for all configuration doorways and is given by Eq. (38c) as

$$\rho_{\text{config}}=\frac{\Gamma_{\text{config}}}{(E_A-E_{\text{con}})^2+(\Gamma_{\text{config}}/2)^2}, \tag{57}$$

where E_{con} is the energy of the degenerate configuration states. We calculate ρ_{config} [and hence $\Gamma^{\text{comp}}_{\text{config}}(d)$] for the cases of $\Gamma_{\text{config}}=1$ and 5 MeV. The former is the value typical of the spreading of a 2p-1h doorway and the latter is a reasonable estimate of the spreading of a single-particle state.[7,8]

TABLE XII. *Total* strengths of all doorway states for each analog resonance in Bi^{209} ($r_C=1.2$ fm).

J^π	E_A (MeV) relative to ground state	$S_{3p-2h}+S_{2p-1h}$ (10^4 keV^2) (Table VII)	S_{config} (10^4 keV^2) (Table IX), $r_C=1.2$ fm	S (10^4 keV^2) Eq. (59)
$\frac{9}{2}^+$	18.57	11.6	28.6	40.2
$\frac{11}{2}^+$	19.36	11.6	27.8	39.4
$\frac{15}{2}^-$	19.98	11.6	32.0	43.6
$\frac{5}{2}^+$	20.14	11.6	33.4	45.0
$\frac{1}{2}^+$	20.60	11.5	46.1	57.6
$\frac{7}{2}^+$	21.07	11.6	30.0	41.6
$\frac{3}{2}^+$	21.11	11.5	42.5	54.0

In Table X the values of $\Gamma^{\text{comp}}_{\text{config}}(d)$ [Eq. (56)] are tabulated (using Table VIII) for all but the antianalog state in columns 2–11 for $\Gamma_{\text{config}}=1$ and 5 MeV. These tabulated compound spreading widths are independent of the spin, parity, and energy of the analog state. In column 1 the range of values of r_C are given and the last two columns give the total compound spreading widths due to these five configuration states.

The total compound spreading width due to all configuration states (including the antianalog) $\Gamma^{\text{comp}}_{\text{config}}$ [Eq. (37c)] may be written using Eq. (55) and the energy degeneracy of the configuration doorways as

$$\Gamma^{\text{comp}}_{\text{config}}=\rho_{\text{config}}S_{\text{config}}. \tag{58}$$

In Table XI for each analog resonance listed in column 1 and for a range of values of r_C (column 3) the values of the compound spreading width due to the antianalog state $\Gamma^{\text{comp}}_{\text{config}}(d=\bar{A})$ are given in columns 4 and 5 for the cases of $\Gamma_{\text{config}}=1$ and 5 MeV, respectively, in Eq. (57). In the last two columns the corresponding total compound spreading widths due to all the configuration doorways $\Gamma^{\text{comp}}_{\text{config}}$ [Eq. (58)] are given. In addition, for each analog state the energy E_{con} is listed in column 2.

5. *Total Compound Spreading Widths and Strengths for all Doorways*

The resulting total strengths and compound mixing widths for a Coulomb radius r_C of 1.2 fm are presented in Tables XII and XIII, respectively.

TABLE XIII. *Total* compound spreading widths due to all doorway states for each analog resonance in Bi^{209} ($r_C=1.2$ fm).

J^π	E_A (MeV) relative to ground state	$\Gamma^{\text{comp}}_{3p-2h}+\Gamma^{\text{comp}}_{2p-1h}$ (keV) (Table VI)	$\Gamma^{\text{comp}}_{\text{config}}$ (keV) (Table XI), $r_C=1.2$ fm Ref. a	Ref. b	Γ^{comp} (keV) Eq. (36) Ref. a	Ref. b
$\frac{9}{2}^+$	18.57	18.6	2.36	11.2	21.0	29.8
$\frac{11}{2}^+$	19.36	19.8	2.30	11.0	22.1	30.8
$\frac{15}{2}^-$	19.98	11.4	2.64	12.6	14.0	24.0
$\frac{5}{2}^+$	20.14	14.3	2.76	13.1	17.1	27.4
$\frac{1}{2}^+$	20.60	12.7	3.81	18.2	16.5	30.9
$\frac{7}{2}^+$	21.07	11.8	2.48	11.8	14.3	23.6
$\frac{3}{2}^+$	21.11	11.5	3.51	16.7	15.0	28.2

[a] $\Gamma_{\text{config}}=1$ MeV in Eq. (57), giving $\rho_{\text{config}}=8.24\times10^{-3}$ MeV^{-1}.

[b] $\Gamma_{\text{config}}=5$ MeV in Eq. (57), giving $\rho_{\text{config}}=3.92\times10^{-2}$ MeV^{-1}.

The total strength S is

$$S = S_{3p-2h} + S_{2p-1h} + S_{config}, \quad (59)$$

where S_{3p-2h}, S_{2p-1h}, and S_{config} are obtained from Eqs. (53), (54), and (55), respectively. In Table XII the first column gives the spin and parity of each analog resonance whose energy (Table III) is given in column 2. Column 3 presents the sum of S_{3p-2h} and S_{2p-1h} (from Table VII), column 4 contains S_{config} (Table IX), and S [Eq. (59)] is presented in the last column. Table XIII shows for each analog resonance indicated in the first two columns the sum $\Gamma^{comp}_{3p-2h} + \Gamma^{comp}_{2p-1h}$ (Table VI) in column 3 and Γ^{comp}_{config} (Table XI) for $\Gamma_{config} = 1$ MeV (5 MeV) in column 4 (5). Finally, the total compound spreading width Γ^{comp} [Eq. (36)] is presented in column 6 (7) for $\Gamma_{config} = 1$ MeV (5 MeV).

6. *Histograms*

In order to study the actual distribution of doorways in terms of their number, matrix-element size, strength, compound mixing width, energy, and density factor we present a number of histograms in Figs. 7–19. The detailed descriptions of the histograms are given in the figure captions. We have selected the $\frac{9}{2}^+$ analog state as typical of the positive-parity analog resonances. In addition, the $\frac{15}{2}^-$ doorway distributions are considered in detail. Figures 7–10 refer to number of states and matrix elements, Figs. 11 and 12 pertain to number of states, strengths, and widths, while Figs. 13–19 relate to energy distributions of the various quantities. Figure 17 is for the case of the $\frac{1}{2}^+$ analog resonance.

IV. DISCUSSION AND CONCLUSIONS

There are several important conclusions that become apparent from the results presented in the preceding section. Among these are:
(1) The calculated spreading widths (of the order of 20 keV, Table XIII) are considerably less than the experimental total widths of the Bi^{209} analog resonances. The latter are of the order of 200–300 keV.[15] The fact that Γ^{comp} is such a small part of the total width is consistent with the Y^{89} results of de Toledo Piza *et al.*[7] and the conclusion of Robson[6] that internal mixing is negligible. The calculated values are also much less than the value of about 80 keV (Mekjian[3] and Lenz and Temmer[23]), which is the estimated spreading width for analogs of lead. The difference is presumably due to the monopole contributions[3] which we have relegated to Γ^{cont} [Eq. (4)] for the purposes of this paper.

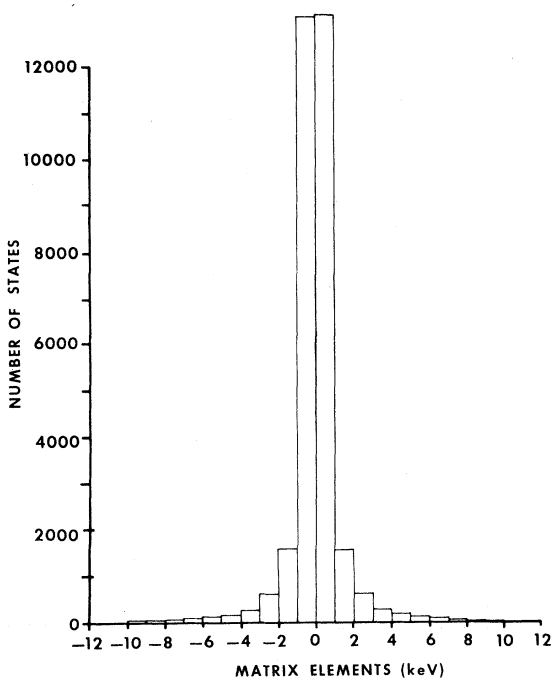

FIG. 7. Histogram of the number of $\frac{9}{2}^+$ doorway states in Bi^{209} vs the valve of the matrix element Eq. (23) for 2p-1h states or Eq. (25) for 3p-2h states (steps of 1 keV). The configuration states are not included.

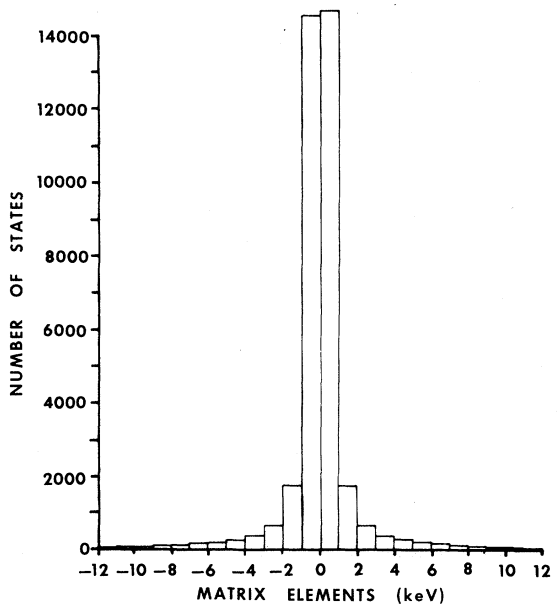

FIG. 8. Histogram of the number of $\frac{15}{2}^-$ doorway states in Bi^{209} vs the value of the matrix element Eq. (23) for 2p-1h states or Eq. (25) for 3p-2h states (steps of 1 keV). The configuration states are not included.

(2) From the histograms (Figs. 15 and 16) in Sec. III it is clear that only certain doorway states have large strengths. These are the configuration states and another set of states in roughly the 20–25-MeV energy range. We shall indicate later that this is the expected energy range of 3p-2h states in Bi^{209} formed from the well-known giant-dipole state in Pb^{208}. In addition to the aforementioned states, important contributors to the compound spreading widths (Figs. 18 and 19) are certain levels of reasonable strength that are very near the analog resonance and consequently possess large density factors (Figs. 13 and 14).
(3) The compound width contributions of the configuration states are about $\frac{1}{8}$ to 1 times that of all other doorways, depending on the value of the configuration spreading width used, i.e., the larger Γ_{config} the greater the value of $\Gamma^{\text{comp}}_{\text{config}}$ (cf. Table XIII).
(4) The relative importance of the antianalog vs other configuration states is strongly dependent on the shell-model position of the single-proton component of the antianalog state (cf. Tables IX–XI, and also Ref. 21).
(5) The strengths (Table VII) of the 2p-1h doorways (Fig. 2) and their compound spreading width contributions (Table VI) are insignificant. Each strength is small primarily because of the very small single-proton amplitude of the analog-state wave function [the $1/\hat{T}$ factor in Eq. (23)]. Also the 2p-1h doorways are in general considerably below the analog resonance, causing the density factors to become almost negligible.
(6) Most 3p-2h doorways have rather small Coulomb matrix elements (Figs. 7–12).
(7) The predicted strengths (Table XII) and compound spreading widths (Table XIII) are roughly the same for all analog states. This reflects the dominance of Pb^{208} intrinsic core contributions over those of the added single nucleon.

We will elaborate on some of these conclusions and discuss additional points of interest in the following paragraphs.

In Table III we note that the $\frac{15}{2}^-$ analog resonance observed in Ref. 15 is slightly lower in energy than the $\frac{5}{2}^+$ analog state, while in Table II the $1j_{15/2}$ single-neutron state is a bit above the $3d_{5/2}$ level. The strengths calculated using the resultant neutron wave functions and the density factors (and hence compound widths) obtained using the energies from Table II would be insignificantly altered if different wave functions and energies (with the $3d_{5/2}$ somewhat above the $1j_{15/2}$) were used. A possible source of error, however, for the $\frac{15}{2}^-$ calculation is that the spectroscopic factor of the $1j_{15/2}$ state is only ≈ 0.5 to 0.6.[4] The spectroscopic factors for the other states are ≈ 1 [4] supporting our single-neutron parent assumption (Fig. 1).

For the quantities calculated in this paper it is essential to know the actual energies and wave functions of the 2p-1h, 3p-2h, and configuration doorways for each analog state. However, if one wishes to know only the total number of 3p-2h states containing a specific neutron hole (Table V), and not the actual ingredients of the 3p-2h states, then the states need be selected [Eq. (24)

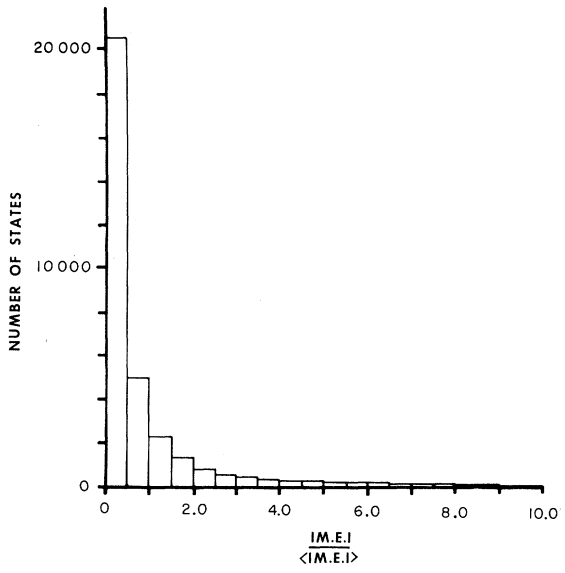

FIG. 9. Histogram of the number of $\frac{9}{2}^+$ doorway states in Bi^{209} vs the ratio of the magnitude of the matrix element to the average value of the magnitude of the matrix element. (Steps of 0.5.) The 2p-1h and 3p-2h matrix elements are given by Eqs. (23) and (25), respectively. The configuration states are not included in computing the average or in the figure.

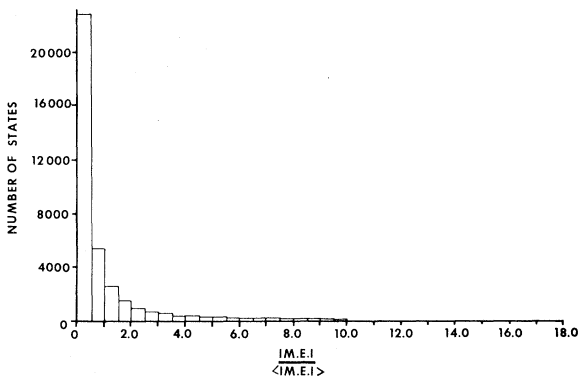

FIG. 10. Histogram of the number of $\frac{15}{2}^-$ doorway states in Bi^{209} vs the ratio of the magnitude of the matrix element to the average value of the magnitude of the matrix element. (Steps of 0.5.) The 2p-1h and 3p-2h matrix elements are given by Eqs. (23) and (25), respectively. The configuration states are not included in computing the average or in the figure.

and Fig. 4] by satisfying the angular momentum coupling rules for only one analog resonance. This is because the number of allowed states for a particular analog resonance depends on the number of allowed values of the intermediate angular momentum I_0 in Fig. 4, and the number of I_0 values will be $2j_h+1$ or $2j'+1$, depending on which is smaller. The spin j' is that of the analog resonance of interest. One can therefore determine the ratio of the number of 3p-2h doorways (containing a certain neutron hole) for one analog state to those of another analog state. For example, the number of possible 3p-2h doorway states having $2f_{7/2}{}^{-1}$ is found to be 7024 for the $\frac{9}{2}^+$ analog resonance (Table V). The ratio of the number of $\frac{9}{2}^+$ 3p-2h doorways containing $2f_{7/2}{}^{-1}$ to the number of $\frac{1}{2}^+$ 3p-2h doorways containing $2f_{7/2}{}^{-1}$ is $[(2\times\frac{7}{2})+1]/[(2\times\frac{1}{2})+1)]=4$. Thus, the number of possible $\frac{1}{2}^+$ 3p-2h doorways having $2f_{7/2}{}^{-1}$ is $\frac{1}{4}\times 7024 = 1756$ (Table V). Since the 3p-2h states (Fig. 4) have more ingredients than the 2p-1h doorways (Fig. 2), there are many more of the former than the latter (Table V).

It is interesting to look at the contribution of a typical 3p-2h state, e.g., one of the 32 312 allowed 3p-2h states for $\frac{9}{2}^+$. Using the notation of Eq. (24) and Fig. 4, a particular doorway is e.g.,

$$|\text{3p-2h}\rangle = |[1h_{9/2}1i_{11/2}(8^-), 1g_{7/2}{}^{-1}; \tfrac{9}{2}^-][2g_{9/2}1h_{9/2}{}^{-1}(2^-)]\tfrac{9}{2}^+\rangle, \quad (60)$$

which is at 22.15 MeV above the ground state (and hence 3.58 MeV above the $\frac{9}{2}^+$ analog resonance) in Bi^{209}. The allowed multipoles k of the Coulomb interaction Eq. (29) are $k=1,\ldots,8$, and the re-

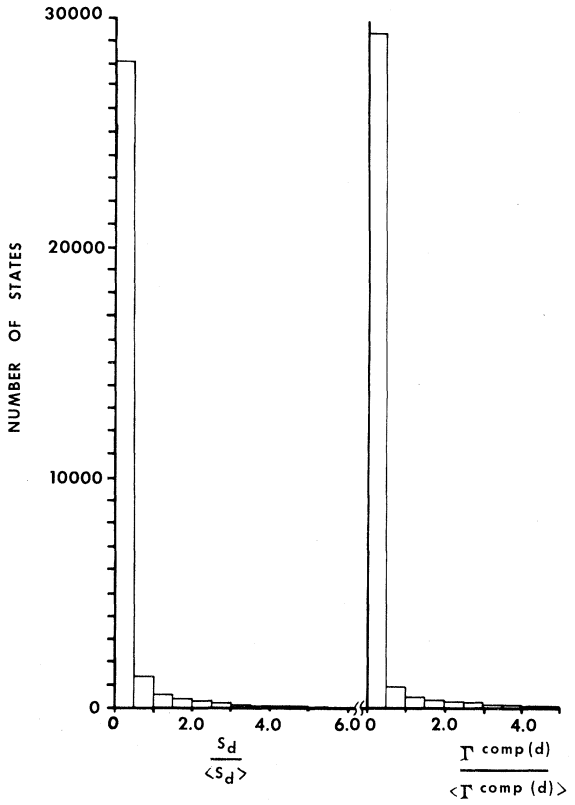

FIG. 11. Histograms of the number of $\frac{9}{2}^+$ doorway states in Bi^{209} vs the ratio of the strength S_d [Eq. (34)] to the average strength $\langle S_d\rangle$ (left-hand side of figure) and vs the ratio of the compound spreading width $\Gamma^{comp}(d)$ to the average compound spreading width $\langle\Gamma^{comp}(d)\rangle$ (right-hand side of figure). The steps are 0.5. The 2p-1h and 3p-2h strengths are given by the squares of Eqs. (23) and (25), respectively, while the 2p-1h and 3p-2h widths are given by $\Gamma^{comp}(d)=\Gamma^{comp}_{2p-1h}(d)$ and $\Gamma^{comp}(d)=\Gamma^{comp}_{3p-2h}(d)$ in Eqs. (37a) and (37b), respectively. The configuration states are not included in computing the average or in the figure.

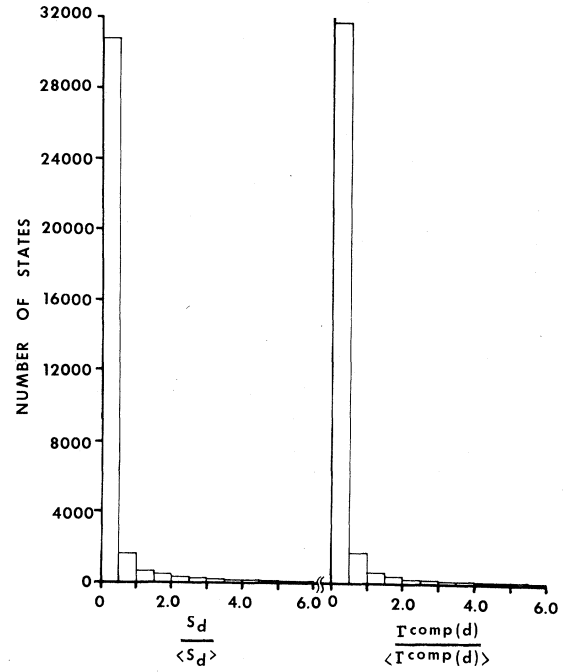

FIG. 12. Histograms of the number of $\frac{15}{2}^-$ doorway states in Bi^{209} vs the ratio of the strength S_d [Eq. (34)] to the average strength $\langle S_d\rangle$ (left-hand side of figure) and vs the ratio of the compound spreading width $\Gamma^{comp}(d)$ to the average compound spreading width $\langle\Gamma^{comp}(d)\rangle$ (right-hand side of figure). The steps are 0.5. The 2p-1h and 3p-2h strengths are given by the squares of Eqs. (23) and (25), respectively, while the 2p-1h and 3p-2h widths are given by $\Gamma^{comp}(d)=\Gamma^{comp}_{2p-1h}(d)$ and $\Gamma^{comp}(d)=\Gamma^{comp}_{3p-2h}(d)$ in Eqs. (37a) and (37b), respectively. The configuration states are not included in computing the average or in the figure.

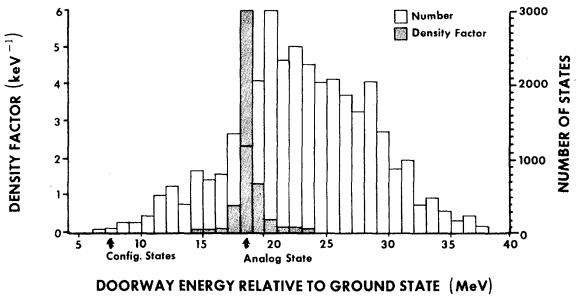

FIG. 13. Histograms of the number of $\frac{9}{2}^+$ doorway states in Bi^{209} and the density factor of the doorways vs the doorway energy relative to the ground state (steps of 1 MeV). The density factor of a doorway is given by Eq. (35) or Eqs. (38a)-(38c). The density factor contribution of the configuration doorways is negligible.

sulting value of the matrix element Eq. (25) is 1.4 keV. (Actually, this is somewhat larger than most 3p-2h matrix elements.) A typical 2p-1h state, e.g., one of the 749 allowed 2p-1h doorways for $\frac{5}{2}^+$ using the notation of Eq. (22) and Fig. 2 is

$$|2\text{p-1h}\rangle = |1h_{9/2}1j_{15/2}(4^+), 2d_{3/2}{}^{-1}; \tfrac{5}{2}^+\rangle, \qquad (61)$$

which is at 12.72 MeV above the ground state (and hence 7.42 MeV below the $\frac{5}{2}^+$ analog resonance) in Bi^{209}. The allowed multipoles k of the Coulomb interaction Eq. (29) are $k=5$ and 7 and the resulting value of the matrix element Eq. (23) is -0.15 keV.

As mentioned in Sec. III B in our work we determine the number of available 3p-2h and 2p-1h states by recording those that can be obtained with the correct total spin and parity from the set of single-particle states of Fig. 6. (For a given set of particles, each different value of J_0 in Fig. 2, or set of values of J_0 and I_0 in Fig. 4, would constitute a different state.) However, there are

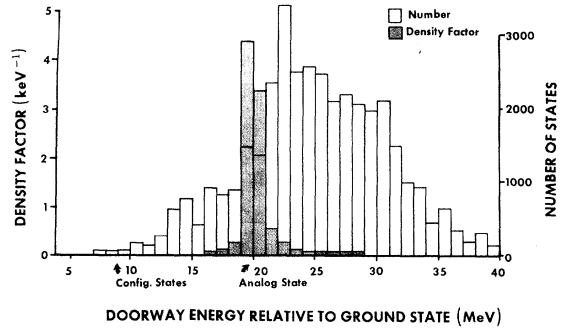

FIG. 14. Histograms of the number of $\frac{15}{2}^-$ doorway states in Bi^{209} and the density factor of the doorways vs the doorway energy relative to the ground state (steps of 1 MeV). The density factor of a doorway is given by Eq. (35) or Eqs. (38a)-(38c). The density factor contribution of the configuration doorways is negligible.

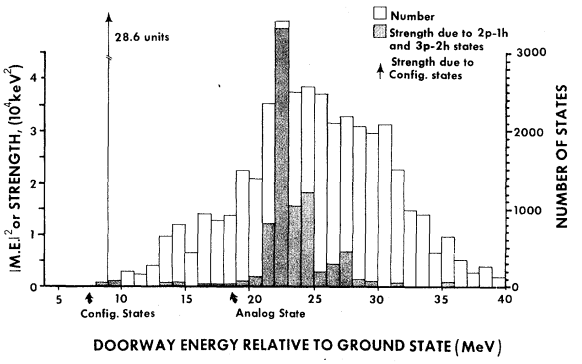

FIG. 15. Histograms of the number of $\frac{9}{2}^+$ doorway states in Bi^{209} and the strength of the doorways vs the doorway energy relative to the ground state (steps of 1 MeV). The strength of a 2p-1h or a 3p-2h doorway is given by the square of Eq. (23) or Eq. (25), respectively. The strength of the antianalog state is given by the square of Eq. (43), while the strength of each other configuration state is given by the square of Eq. (44).

a very small number of doorway states for which the two-body Coulomb matrix element is identically zero, there being no multipole order k to satisfy Eq. (29). A typical such state is

$$|1h_{9/2}2f_{7/2}(1^+)3s_{1/2}{}^{-1}, \tfrac{1}{2}^+\rangle.$$

We include such states on our counting. In addition, there are a few states for which $k=0$ is possible in the two-body Coulomb expansion. (These are not to be confused with the giant-monopole state discussed by Mekjian.[3]) One such state is $|[2f_{5/2}3d_{3/2}(3^-), 2d_{3/2}{}^{-1}; \tfrac{5}{2}^-][2g_{9/2}2f_{5/2}{}^{-1}(2^-)]\,\tfrac{9}{2}^+\rangle$.

Figures 7 and 8 show via histograms (for all but the configuration doorways) that positive- and negative-value Coulomb matrix elements are equally

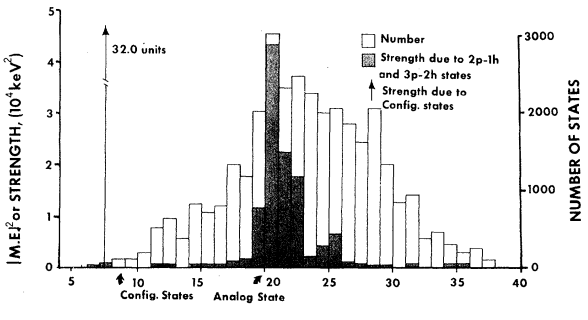

FIG. 16. Histograms of the number of $\frac{15}{2}^-$ doorway states in Bi^{209} and the strength of the doorways vs the doorway energy relative to the ground state (steps of 1 MeV). The strength of a 2p-1h or a 3p-2h doorway is given by the square of Eq. (23) or Eq. (25), respectively. The strength of the antianalog state is given by the square of Eq. (43), while the strength of each other configuration state is given by the square of Eq. (44).

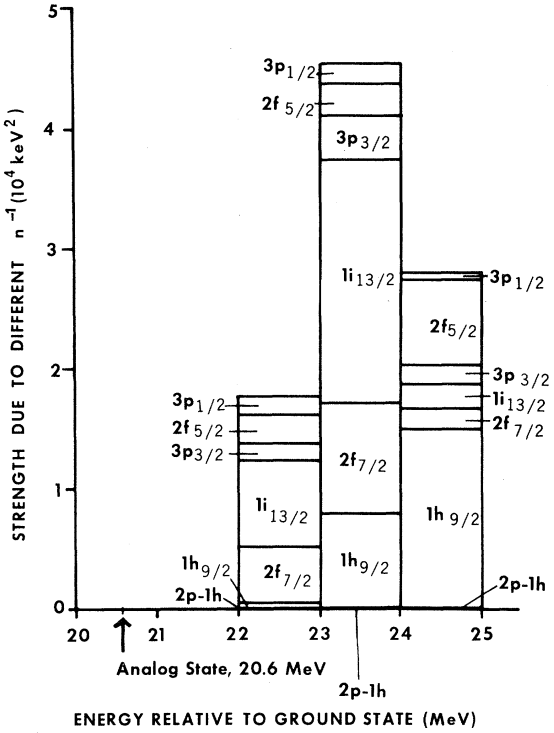

FIG. 17. Histogram of the strength of $\frac{1}{2}^+$ doorway states in Bi^{209} between 22 and 25 MeV vs the doorway energy relative to the ground state (steps of 1 MeV). The strength of a 2p-1h or a 3p-2h doorway is given by the square of Eq. (23) or Eq. (25), respectively. For the 3p-2h doorways the contribution from those states containing a particular neutron hole is indicated.

likely. This is just a verification of the usual random-phase approximation made quite often in physics. We are really interested in the square of matrix elements rather than their signs; however, Figs. 7 and 8 serve, because of their symmetry about 0 keV, as good checks on the accuracy of our computer program. While it is not shown, the analogous $\frac{1}{2}^+$ histogram is slightly less symmetric than the $\frac{9}{2}^+$ histogram (Fig. 7) because there are about $\frac{1}{4}$ as many $\frac{1}{2}^+$ as there are $\frac{9}{2}^+$ doorway states to be sampled (Table V).

While the histograms (Figs. 7–19) are for $\frac{9}{2}^+$ and $\frac{15}{2}^-$ (except for Fig. 17) the results are similar for the other analog resonances. Most matrix elements (Figs. 7 and 8) are less than 1 *keV* in magnitude. This is to be compared with the gross Coulomb energy shift C [Eq. (39) and Table II] of about 19 *MeV*. Configuration state matrix elements can be of the order of *several hundred keV*. (This can be inferred from the square roots of the strengths in Tables VIII, IX, and XII; see also Ref. 21.) Nevertheless, the 3p-2h doorways contribute a total strength for each analog resonance of about $\frac{1}{3}$ that due to the six configuration states (Table XII). This is due to the fact that there are *many thousands* of the small 3p-2h matrix elements contributing. While the configuration state strengths in Table XII are larger than those of the other doorways, the situation is reversed for the compound spreading widths evaluated at $\Gamma_{\text{config}} = 1$ MeV (Table XIII). This is because of the large value of $E_{\text{sym}} = 11$ MeV which results in a rather small density factor.

In Figs. 9 through 12 we note that the distributions of the number of states are peaked at very small values of the abscissa (less than 0.5). In particular Figs. 9 and 10 relate to $|\text{M.E.}|/\langle\text{M.E.}\rangle$,

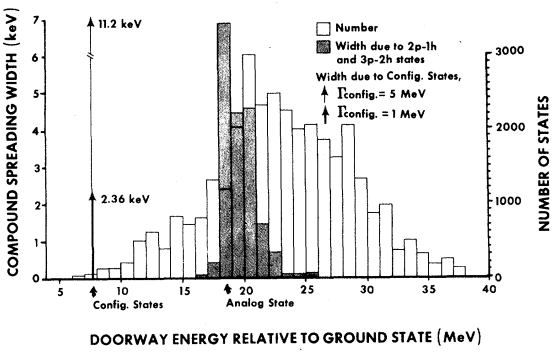

FIG. 18. Histograms of the number of $\frac{9}{2}^+$ doorway states in Bi^{209} and the compound spreading width of the doorways vs the doorway energy relative to the ground state (steps of 1 MeV). The widths $\Gamma^{\text{comp}}_{2p-1h}(d)$, $\Gamma^{\text{comp}}_{3p-2h}(d)$, and $\Gamma^{\text{comp}}_{\text{config}}(d)$ are indicated in Eqs. (37a)–(37c), respectively.

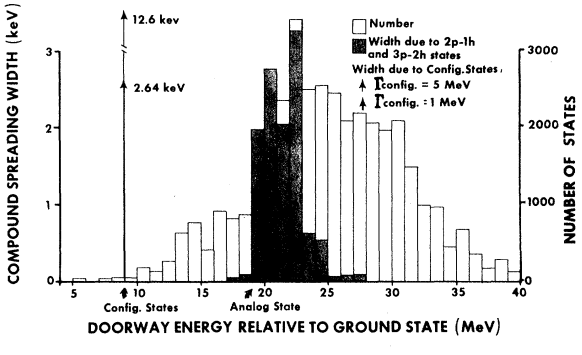

FIG. 19. Histograms of the number of $\frac{15}{2}^-$ doorway states in Bi^{209} and the compound spreading width of the doorways vs the doorway energy relative to the ground state (steps of 1 MeV). The widths $\Gamma^{\text{comp}}_{2p-1h}(d)$, $\Gamma^{\text{comp}}_{3p-2h}(d)$, and $\Gamma^{\text{comp}}_{\text{config}}(d)$ are indicated in Eqs. (37a)–(37c), respectively.

and Figs. 11 and 12 to both $S_d/\langle S_d\rangle$ and $\Gamma^{\rm comp}(d)/\langle\Gamma^{\rm config}(d)\rangle$. The shapes of these histograms are reminiscent of the Porter-Thomas distributions often observed in low-energy neutron scattering experiments.

As mentioned in Sec. III B 3 it is clear from Table VII that $S_{3p-2h}(h)$ is independent of the spin and parity of the analog resonance. This is reasonable since the neutron hole is in the Pb^{208} core and is independent of the added nucleon; however, in squaring Eq. (25) a factor of $1/(2J+1)$ appears which indicates a dependence on the spin and parity of the analog resonance and hence on the added nucleon. This contradiction is removed by realizing that $S_{3p-2h}(h)$ is the sum of the squares of many matrix elements [Eq. (52)]. For a given set of five quasiparticles the strength is proportional to $\sum_{I_0}(2I_0+1)$ [cf. Eq. (25)], and since $\vec{j}_h+\vec{J}=\vec{I}_0$, we have

$$\sum_{I_0}(2I_0+1)=(2j_h+1)(2J+1)\,, \tag{62}$$

so that the factor of $(2J+1)$ cancels the aforementioned factor of $1/(2J+1)$.

Because their wave functions have no single-proton components the configuration states (Table IV) other than the antianalog have strengths (Table VIII) independent of the spin and parity of the analog resonance. In Table VIII the contributions due to $\bar{A}_2$ and $\bar{A}_4$ are quite small because of our choice of coupling in generating the configuration state wave functions. We see in Table VIII a strong dependence on the Coulomb radius r_C. It is therefore necessary to choose a reliable value of r_C and Ref. 22 indicates that this is 1.2 fm. The strength at various radii is shown in Table IX for the antianalog state. Here, there is as expected, a noticeable dependence not only on r_C, but also (because of the single-proton component, Table IV) on the spin and parity of the analog state. This latter dependence may be understood from the matrix element Eq. (45). If the wave function of the single proton $|p\rangle$ is quite different from those of the protons in the quantum states of the excess neutrons, then the magnitude of $\langle p|V_C(r)|p\rangle$ will be quite different from the sizes of the matrix elements involving the other protons in Eq. (45). In particular, each of the latter should be larger than $\langle p|V_C(r)|p\rangle$ because those protons are on the average closer to the nucleus and hence feel more Coulomb repulsion. The result of this is that the amount of cancellation in Eq. (45) will be decreased. In Table IX the $\frac{1}{2}^+$ analog resonance illustrates this, the $4s_{1/2}$ state having a much different wave function (because of $n=4$) than all the other protons.

The widths $\Gamma^{\rm comp}_{\rm config}(\bar{A}_i)$ in Table X are independent of the analog-state spin and parity because the number of configuration states is the same for all analog resonances, and the density factors for all analog states are the same Eq. (57). It is clear from Eqs. (57) and (58) that the result of having $\Gamma_{\rm config}$ in the numerator of Eq. (57) is to strongly affect $\Gamma^{\rm comp}_{\rm config}$. This is manifested by the numbers tabulated in the last two columns of Tables X and XI. The components of the configuration state wave functions are all 2p-1h except for the antianalog state (Table IV), and but for the $\frac{1}{2}^+$ and $\frac{3}{2}^+$ (and perhaps $\frac{5}{2}^+$) analog states the contributions from the antianalog states are not very important (Table XI). Therefore $\Gamma_{\rm config}=1$ MeV is more reasonable than $\Gamma_{\rm config}=5$ MeV, which is characteristic of single-particle states. In any event we would expect the parameter $\Gamma_{\rm config}$ to be nearer 1 MeV than 5 MeV, and the numbers in the columns labeled Ref. a in Table XIII to be good rough estimates of upper limits for the compound mixing widths in Bi^{209}.

In Figs. 13 and 14 we note that the distributions of states for $\frac{9}{2}^+$ and $\frac{15}{2}^-$ are similar and that most available states are energetically above the analog state. Near the configuration states, while there are relatively few doorways, there are nevertheless enough to provide for nuclear damping. This damping is manifested in the spreading width parameter $\Gamma_{\rm config}$. It is clear from these figures that the region of large density factors covers about 1 to 2 MeV on either side of the analog state.

The histograms in Figs. 15 and 16 graphically show the distributions of strengths that lead to the summaries given in Table XII. We see that from all the many thousands of states the strength comes primarily (as mentioned earlier) from two main sources, viz., the configuration states and a set of states near about 22 MeV. The latter group consists essentially of those states for which $k=1$ (the dipole term) in the Coulomb expansion [Eqs. (28) and (29)] is allowed. Since the Coulomb interaction is long range, we expect the lowest multipoles to contribute most strongly. The dipole term is a manifestation of this. What we are most probably calculating are the effects of these 3p-2h doorways whose common origin is the well-known giant-dipole state at about 14 MeV in Pb^{208}. While it is difficult to actually predict the correct energy of the Pb^{208} dipole resonance,[24-26] the wave function is most likely primarily of the particle-hole type. The subsequent addition of various sets of two particles and a hole to this state yields doorways in the 20–25-MeV range (cf. the energies in Table II) that are by virtue of their construction generically related to the giant dipole resonance. Such a doorway is for example, the 3p-2h state given in Eq. (60). The large (and

hence very important) matrix elements (extending to about 10–12 keV) in Figs. 7 and 8 are also of the general type described above.

In Fig. 17 we show the basic makeup of the doorway states in the dipole energy range for the $\frac{1}{2}^+$ analog resonance. The overwhelming strength contributions come from 3p-2h states, and the histogram indicates how the strengths for the various neutron holes (cf. Table VII) are distributed.

Finally, Figs. 18 and 19 show the distributions of widths that lead to the compound spreading widths presented in Table XIII. The major contributions from the nonconfiguration doorways are shifted to the left slightly from the dominant strengths in Figs. 15 and 16. This is the influence of the large density factors shown in Figs. 13 and 14, and this effect is summarized in conclusion 2 of this section.

It would be of interest in a future calculation to use a particle-vibration model for the doorways, especially those of dipole origin. While such a model would eliminate much of the microscopic information and detail presented here, it would more clearly convey the general collective doorway behavior.

One of us (W.P.B.) acknowledges very useful discussions during the course of this work with Professor A. Kerman and Professor C. Shakin and an early discussion with Dr. A. F. R. de Toledo Piza. We are grateful to Dr. David Tanner for helping us with several computer problems and we thank Nick Schneiders for his help in plotting the histograms.

---

*The final stage of this work and the writing of the manuscript were supported in part by the U. S. Army Research Office, Durham, North Carolina.

[1]*Isobaric Spin in Nuclear Physics,* edited by J. Fox and D. Robson (Academic, New York, 1966); *Nuclear Isospin,* edited by J. D. Anderson, S. D. Bloom, J. Cerny, and W. W. True (Academic, New York, 1969); *Isospin in Nuclear Physics,* edited by D. H. Wilkinson (North-Holland, Amsterdam, 1969).

[2]A. K. Kerman, in *Nuclear Isospin,* edited by J. D. Anderson, S. D. Bloom, J. Cerny, and W. W. True (Academic, New York, 1969), p. 315.

[3]A. Z. Mekjian, Phys. Rev. Letters 25, 888 (1970).

[4]N. Auerbach, J. Hüfner, A. K. Kerman, and C. M. Shakin, Rev. Mod. Phys. 44, 48 (1972).

[5]A. F. R. de Toledo Piza and A. K. Kerman, Ann. Phys. (N.Y.) 43, 3 (1967).

[6]D. Robson, Phys. Rev. 137, B535 (1965).

[7]A. F. R. de Toledo Piza, A. K. Kerman, S. Fallieros, and R. H. Venter, Nucl. Phys. 89, 369 (1966).

[8]A. Z. Mekjian, Phys. Rev. 184, 1031 (1969).

[9]D. Robson, in *Nuclear Isospin,* edited by J. D. Anderson, S. D. Bloom, J. Cerny, and W. W. True (Academic, New York, 1969), p. 385.

[10]J. Blomqvist and S. Wahlborn, Arkiv Fysik 16, 545 (1960).

[11]D. A. Bromley and J. Weneser, Comments Nucl. Particle Phys. 2, 151 (1968).

[12]N. Stein, in *Proceedings of the International Conference on Properties of Nuclear States, Montreal, Canada, 1969,* edited by M. Harvey *et al.* (Presses de L'Université de Montréal, Montréal, Canada, 1969), p. 337.

[13]W. T. Pinkston, Nucl. Phys. 53, 643 (1964).

[14]S. Fallieros, J. Franklin Inst. 281, 179 (1966).

[15]W. R. Wharton, P. Von Brentano, W. K. Dawson, and P. Richard, Phys. Rev. 176, 1424 (1968).

[16]M. H. MacFarlane and J. P. Schiffer, Comments Nucl. Particle Phys. 3, 107 (1969).

[17]A. Z. Mekjian, Nucl. Phys. A146, 288 (1970).

[18]I. Hamamoto, Nucl. Phys. A141, 1 (1970).

[19]A. H. Wapstra, Handbuch der Physik 38, 1 (1958).

[20]E. H. Auerbach, BNL Report No. 6562, 1962 (unpublished).

[21]W. P. Beres and D. Voges, to be published.

[22]J. A. Nolen and J. P. Schiffer, Ann. Rev. Nucl. Sci. 19, 471 (1969).

[23]G. H. Lenz and G. M. Temmer, Nucl. Phys. A112, 625 (1968).

[24]V. Gillet, A. M. Green, and E. H. Sanderson, Nucl. Phys. 88, 321 (1966).

[25]T. T. S. Kuo, J. Blomqvist, and G. E. Brown, Phys. Letters 31B, 93 (1970).

[26]S. M. Perez, Phys. Letters 33B, 317 (1970).

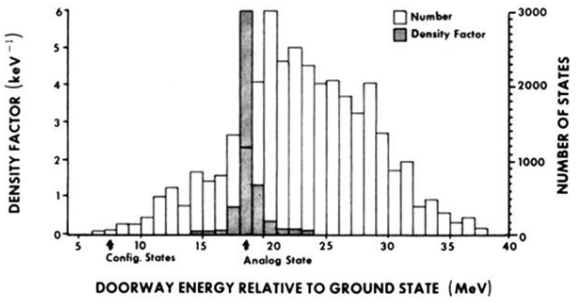

FIG. 13. Histograms of the number of $\frac{9}{2}^+$ doorway states in Bi^{209} and the density factor of the doorways vs the doorway energy relative to the ground state (steps of 1 MeV). The density factor of a doorway is given by Eq. (35) or Eqs. (38a)-(38c). The density factor contribution of the configuration doorways is negligible.

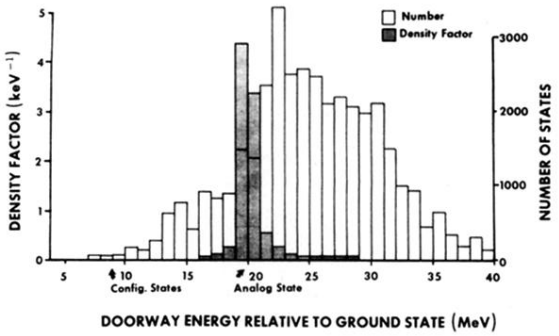

FIG. 14. Histograms of the number of $\frac{15}{2}^-$ doorway states in Bi^{209} and the density factor of the doorways vs the doorway energy relative to the ground state (steps of 1 MeV). The density factor of a doorway is given by Eq. (35) or Eqs. (38a)-(38c). The density factor contribution of the configuration doorways is negligible.

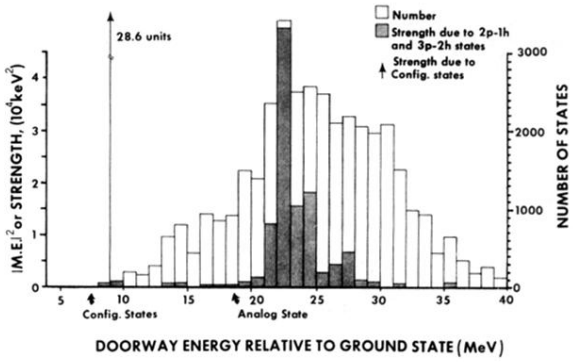

FIG. 15. Histograms of the number of $\frac{9}{2}^+$ doorway states in Bi^{209} and the strength of the doorways vs the doorway energy relative to the ground state (steps of 1 MeV). The strength of a 2p-1h or a 3p-2h doorway is given by the square of Eq. (23) or Eq. (25), respectively. The strength of the antianalog state is given by the square of Eq. (43), while the strength of each other configuration state is given by the square of Eq. (44).

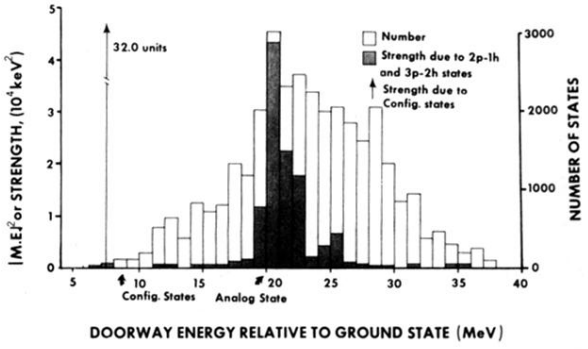

FIG. 16. Histograms of the number of $\frac{15}{2}^-$ doorway states in Bi^{209} and the strength of the doorways vs the doorway energy relative to the ground state (steps of 1 MeV). The strength of a 2p-1h or a 3p-2h doorway is given by the square of Eq. (23) or Eq. (25), respectively. The strength of the antianalog state is given by the square of Eq. (43), while the strength of each other configuration state is given by the square of Eq. (44).

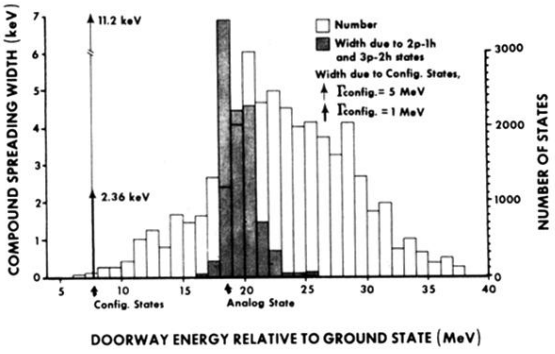

FIG. 18. Histograms of the number of $\frac{9}{2}^+$ doorway states in Bi^{209} and the compound spreading width of the doorways vs the doorway energy relative to the ground state (steps of 1 MeV). The widths $\Gamma^{\text{comp}}_{2p-1h}(d)$, $\Gamma^{\text{comp}}_{3p-2h}(d)$, and $\Gamma^{\text{comp}}_{\text{config}}(d)$ are indicated in Eqs. (37a)–(37c), respectively.

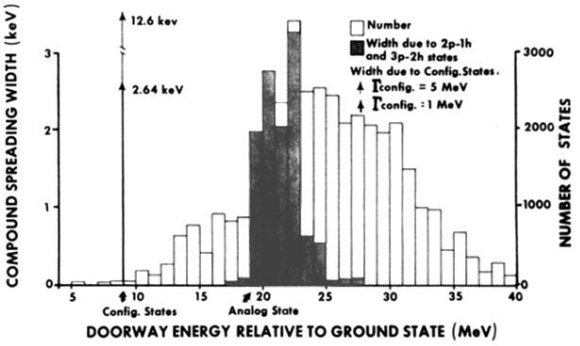

FIG. 19. Histograms of the number of $\frac{15}{2}^-$ doorway states in Bi^{209} and the compound spreading width of the doorways vs the doorway energy relative to the ground state (steps of 1 MeV). The widths $\Gamma^{\text{comp}}_{2p-1h}(d)$, $\Gamma^{\text{comp}}_{3p-2h}(d)$, and $\Gamma^{\text{comp}}_{\text{config}}(d)$ are indicated in Eqs. (37a)–(37c), respectively.